Hα FLUORESCENCE IN UV ACTIVE BINARY STARS

By

TODD RUSSELL VACCARO

A DISSERTATION PRESENTED TO THE GRADUATE SCHOOL
OF THE UNIVERSITY OF FLORIDA IN PARTIAL FULFILLMENT
OF THE REQUIREMENTS FOR THE DEGREE OF
DOCTOR OF PHILOSOPHY

UNIVERSITY OF FLORIDA

2001

ACKNOWLEDGMENTS

I would like to thank my advisor for all the assistance and guidance he has given me over the past few years, especially for going on a 12 night observing run and obtaining the photometry used in this work. We would like to thank the Kitt Peak National Observatory and the Southeastern Association for Research in Astronomy for giving us the telescope time. We are especially grateful for the observing support of Walter Van Hamme, Rolando Branley, Peter Mack, and Gerrie Peters.

I am grateful to my graduate committee members for taking the time out to perform this duty.

I would like to thank the Department of Astronomy for the teaching assistantships that have mostly supported me during my time here at the University of Florida and for the financial assistance in traveling to some of the meetings I have attended.

I am especially grateful to my wife, Paula, whose love, patience, support, and devotion have all made this possible.

TABLE OF CONTENTS

ACKNOWLEDGMENTS ii

LIST OF TABLES iv

LIST OF FIGURES v

ABSTRACT viii

CHAPTERS

1 INTRODUCTION 1

1.1 The Study of Binary Stars 1
1.2 UV Active Binary Stars and Fluorescence 1

2 THE SCIENTIFIC STRATEGY 4

2.1 The Models 4
2.2 The Candidate Systems 9

3 THE DATA 12

3.1 Our Observations 12
3.2 Photometry 12
3.3 Spectroscopy 14

4 THE ANALYSIS 16

4.1 FF Aqr 16
4.2 V471 Tau 31

5 CONCLUSION 78

REFERENCES 80

BIOGRAPHICAL SKETCH 82

LIST OF TABLES

3.1 Photometric coverage. 14
3.2 Radial velocity lines. 14
4.1 FF Aqr parameter solutions. 18
4.2 FF Aqr spot solutions. 19
4.3 V471 Tau parameter solutions. 34
4.4 V471 Tau spot parameters. 34

LIST OF FIGURES

2.1 Model light curves: ellipsoidal effects (top) and ellipsoidal combined with reflection effects (bottom). 5

2.2 The Hα profile model of the back side of the star (eclipse). 9

2.3 The Hα profile model showing the fluorescing region rotating into view (phase=0.30). 9

2.4 The Hα profile model with fluorescing region in full view (phase=0.50). 10

4.1 The model radial velocity curve (solid line) and our observed velocities (points). 19

4.2 Our model light curve (solid line) and photometric measurements (points) extracted from the phase plot in the literature. 20

4.3 Scaled pictures of FF Aqr that show the spots used in our models. Images were made with the WD program. 22

4.4 Light curve models with WD (solid line) compared with our photometry (dots) in each color observed. 23

4.5 The model radial velocity curve, which includes spots (solid line) and our observed velocities (points). 24

4.6 Observed spectrum of FF Aqr at ϕ=0.52 (solid line) and the modeled Fe line at 6400Å (dashed line). 24

4.7 Observed spectra of FF Aqr (dots) and the modeled Hα profile (solid line) for phases 0.06-0.28. 26

4.8 Observed spectra of FF Aqr (dots) and the modeled Hα profile (solid line) for phases 0.30-0.52. 27

4.9 Observed spectra of FF Aqr (dots) and the modeled Hα profile (solid line) for phases 0.63-0.95. 28

4.10 The model radial velocity curve (solid line) and our observed velocities (points). 33

4.11 Scaled pictures of V471 Tau that show the spots used in our models. Images were made with the WD program. 36

4.12 Light curve models with WD (solid line) compared with our photometry (dots) in each color observed. 37

4.13 Observed spectra of V471 Tau (symbols) and the modeled Hα profile (solid line) for phases 0.00-0.01. 38

4.14 Observed spectra of V471 Tau (symbols) and the modeled Hα profile (solid line) for phases 0.03-0.04. 40

4.15 Observed spectra of V471 Tau (symbols) and the modeled Hα profile (solid line) for phases 0.07-0.08. 41

4.16 Observed spectra of V471 Tau (symbols) and the modeled Hα profile (solid line) for phases 0.09-0.10. 42

4.17 Observed spectra of V471 Tau (symbols) and the modeled Hα profile (solid line) for phases 0.12-0.14. 43

4.18 Observed spectra of V471 Tau (symbols) and the modeled Hα profile (solid line) for phases 0.16-0.17. 44

4.19 Observed spectra of V471 Tau (symbols) and the modeled Hα profile (solid line) for phases 0.18-0.20. 45

4.20 Observed spectra of V471 Tau (symbols) and the modeled Hα profile (solid line) for phases 0.21-0.22. 46

4.21 Observed spectra of V471 Tau (symbols) and the modeled Hα profile (solid line) for phases 0.23-0.24. 47

4.22 Observed spectra of V471 Tau (symbols) and the modeled Hα profile (solid line) for phases 0.25-0.29. 48

4.23 Observed spectra of V471 Tau (symbols) and the modeled Hα profile (solid line) for phases 0.30-0.31. 49

4.24 Observed spectra of V471 Tau (symbols) and the modeled Hα profile (solid line) for phases 0.33-0.35. 50

4.25 Observed spectra of V471 Tau (symbols) and the modeled Hα profile (solid line) for phases 0.36-0.37. 51

4.26 Observed spectra of V471 Tau (symbols) and the modeled Hα profile (solid line) for phases 0.39-0.40. 52

4.27 Observed spectra of V471 Tau (symbols) and the modeled Hα profile (solid line) for phases 0.41-0.42. 53

4.28 Observed spectra of V471 Tau (symbols) and the modeled Hα profile (solid line) for phases 0.43-0.45. 54

4.29 Observed spectra of V471 Tau (symbols) and the modeled Hα profile (solid line) for phases 0.46-0.47. 55

4.30 Observed spectra of V471 Tau (symbols) and the modeled Hα profile (solid line) for phases 0.48-0.49. 56

4.31 Observed spectra of V471 Tau (symbols) and the modeled Hα profile (solid line) for phases 0.50-0.51. 57

4.32 Observed spectra of V471 Tau (symbols) and the modeled Hα profile (solid line) for phases 0.52-0.53. 61

4.33 Observed spectra of V471 Tau (symbols) and the modeled Hα profile (solid line) for phases 0.54-0.58. 62

4.34 Observed spectra of V471 Tau (symbols) and the modeled Hα profile (solid line) for phases 0.60-0.61. 63

4.35 Observed spectra of V471 Tau (symbols) and the modeled Hα profile (solid line) for phases 0.62-0.64. 64

4.36 Observed spectra of V471 Tau (symbols) and the modeled Hα profile (solid line) for phases 0.65-0.67. 65

4.37 Observed spectra of V471 Tau (symbols) and the modeled Hα profile (solid line) for phases 0.68-0.69. 66

4.38 Observed spectra of V471 Tau (symbols) and the modeled Hα profile (solid line) for phases 0.71-0.72. 67

4.39 Observed spectra of V471 Tau (symbols) and the modeled Hα profile (solid line) for phases 0.73-0.75. 68

4.40 Observed spectra of V471 Tau (symbols) and the modeled Hα profile (solid line) for phases 0.76-0.77. 69

4.41 Observed spectra of V471 Tau (symbols) and the modeled Hα profile (solid line) for phases 0.78-0.80. 70

4.42 Observed spectra of V471 Tau (symbols) and the modeled Hα profile (solid line) for phases 0.81-0.82. 71

4.43 Observed spectra of V471 Tau (symbols) and the modeled Hα profile (solid line) for phases 0.84-0.86. 72

4.44 Observed spectra of V471 Tau (symbols) and the modeled Hα profile (solid line) for phases 0.89-0.90. 73

4.45 Observed spectra of V471 Tau (symbols) and the modeled Hα profile (solid line) for phases 0.91-0.92. 74

4.46 Observed spectra of V471 Tau (symbols) and the modeled Hα profile (solid line) for phases 0.93-0.94. 75

4.47 Observed spectra of V471 Tau (symbols) and the modeled Hα profile (solid line) for phases 0.95-0.96. 76

4.48 Observed spectra of V471 Tau (symbols) and the modeled Hα profile (solid line) for phases 0.97-0.99. 77

Abstract of Dissertation Presented to the Graduate School
of the University of Florida in Partial Fulfillment of the
Requirements for the Degree of Doctor of Philosophy

Hα FLUORESCENCE IN UV ACTIVE BINARY STARS

By

Todd Russell Vaccaro

May 2001

Chairman: Dr. Robert E. Wilson
Major Department: Astronomy

Light curves, radial velocity curves, and Hα spectral profile models were generated for the eclipsing binaries V471 Tau and FF Aqr. We modeled an emission region on the cool star of each system to simulate fluorescent activity on the side of the star facing its hot companion. Comparisons of the models to our photometric and spectroscopic observations reveal additional components that may arise from the intrinsic chromospheric activity of the cooler star and be associated with dark spotted regions. More emissions were found at higher velocities that place the activity well above the star but still between the two stars. The sources of these excess emissions may be extended structures such as prominences, a partially ionized wind, or circumstellar material such as a ring or disk. The combined emissions greatly complicate a formerly simple illumination model.

CHAPTER 1
INTRODUCTION

1.1 The Study of Binary Stars

The Sun is the only star from which we can measure fundamental stellar properties with high accuracy. Knowledge of its mass, size, and luminosity along with its internal and external physical processes allows us to trace its history, understand its current state, and predict its future. Yet there are observations that still elude detailed explanations, such as the magnetic activity cycle, which has been seen on the photosphere at least since the time of Galileo. Ability to discover more about stellar physics comes from the study of binary stars with similar activities.

Short period binaries offer a wealth of information about the orbital motion of the stars as well as any cycle-to-cycle variations that may exist. Direct visual observations of the individual stars or their motions cannot be made in such binaries; therefore surface features are determined photometrically while radial velocities must be measured spectroscopically. Spectroscopy can also yield information about temperature, rotation, chemical abundances, and physical details of the surrounding environment, such as gas streams, winds, disks, shells, and extended structures (flares, prominences, etc.). Further supporting data can be obtained photometrically if the orbital plane is highly inclined to the plane of the sky. These systems yield accurate orbital periods by eclipse timing and provide information on relative stellar sizes via eclipse depths and durations.

1.2 UV Active Binary Stars and Fluorescence

A veritable zoo of binary types exists. Categories are based on the types of stellar components, on activities, and on evolutionary states. A broad morphological

categorization bases close systems on limiting lobes (Roche lobes) of equipotential surfaces that surround both stars. These lobes are regions that limit the sizes of the stars while maintaining hydrostatic equilibrium. The lobe size relative to the orbital separation is a function of mass ratio, rotation rate, and orbital eccentricity. The filling of these lobes by the stars leads to 4 basic configurations: *detached*, *semi-detached*, *overcontact* and *double contact*. Detached binaries have both stars inside their limiting lobes. Co-rotating material on or immediately surrounding each star is then gravitationally bound to that star. One star fills its lobe in a semi-detached system. There exists a saddle point between the stars that becomes a site of mass transfer where gas can freely fall towards its companion when a lobe is filled. Overcontact binaries have both stars overfilling their limiting lobes. Evolutionary effects could cause a filling of the lobes via stellar expansion or orbital shrinkage, which constricts the lobes about each star. Stable systems of all four kinds can be found. Algols and novae (cataclysmic variables) are examples of the semi-detached variety while W UMa binaries exemplify the overcontact kind. The double contact stars are discussed by Wilson (1979). These binaries are complicated by mass transfer. Detached systems are not complicated by rapid or streaming mass transfer. Some possible effects occurring in these binaries are tidal locking of rotation with the orbit (*ie.* synchronous rotation), heating of facing hemispheres (*ie.* reflection effect), wind interaction, and fluorescence. Synchronous rotation is commonly found in most small circular orbits, along with some lobe filling, due to the nature of tides.

Our term of *UV active binaries* is a general designation. The ultra-violet source in this case is a hot primary component that may be a white dwarf or sub-dwarf star. The secondary component is a cooler star that shows enhanced solar-like activity. Dark spots, bright plages, and some flares are detectable by photometric observations. The increased activity of the secondary is due to its rapid rotation which is tidally induced by the small orbit. The binaries exist in a detached state;

thereby providing a UV point source as a probe for the otherwise unaffected secondary and a system free of mass transfer effects.

These systems offer a unique opportunity to study the secondary's UV irradiated atmosphere. The disparity in stellar sizes accounts for the secondary's overwhelming luminosity, so it is easy to observe at long wavelengths without contamination from the hot blue primary. Eclipsing systems of this type provide two distinct aspects of the secondary, that of the star itself during primary eclipse and that of an illuminated region during inferior conjunction of the primary. The cool star's chromosphere is optically thick to the incident UV radiation. The effect is ionization of hydrogen in this layer with subsequent recombination and emission (*i.e.*, fluorescence). The red Balmer line of Hα is one of the strongest lines produced in this process, well isolated from the white dwarf's light in the visual range, and easily observed from the ground. The line should vary regularly in strength and profile as the illuminated hemisphere rotated in and out of sight.

Modeling this fluorescence is a step in understanding the radiative processes in another star's chromosphere. It is a permanent feature that should be seen from cycle to cycle. However there are additional emissions that are intrinsic to the secondary. Emission lines of CaII(H + K), MgII(h + k), and Hα are clear indicators of an active chromosphere (Bopp & Talcott 1980). The mechanisms for these emissions could be linked to magnetic structures such as dark photospheric spots or plages (Young, Skumanich, & Paylor 1988). These regions are known to be activity centers for events, such as flares and prominences, which would wax and wane in strength and frequency like those observed for the sunspot cycle.

CHAPTER 2
THE SCIENTIFIC STRATEGY

2.1 The Models

Our approach for identifying and modeling fluorescence in candidate binaries requires Hα spectroscopy with simultaneous photometric coverage over one or more entire orbits. The spectroscopy provides us with the behavior of the Hα line at various phases. Wave distortions in the light curves reveal locations of spot regions. Spots are known sites of activity and can be modeled as additional sources of steady or flaring emission that can help explain spectroscopic anomalies. Orbital and binary parameters are also derived by combining radial velocities with the light curves.

Model light curves, radial velocity curves, and spectral profiles are all made with the WD program (Wilson and Devinney, 1971; Wilson, 1979; 1990). Light curves are made by integrating emergent flux over a finite grid of surface elements. The elements are positioned on the surface equipotentials in polar coordinates for each star by the equation

$$\Omega = r^{-1} + q[(1 - 2\lambda r + r^2)^{-\frac{1}{2}} - \lambda r] + \frac{1}{2}(q+1)r^2(1-\nu^2),$$

were $q = \frac{m_2}{m_1}$ and λ , ν are direction cosines. The equation is solved for $r(\theta, \phi, q, \Omega)$ by the Newton-Raphson method. The relative brightness (*light*) is computed by integrating the emergent flux over all the visible elements. The program accounts for horizon and eclipse effects as well as gravity brightening, limb darkening, and reflection effects. The eclipsing binary FF Aqr is used as an example of these effects in Figure 2.1. The first panel shows the ellipsoidal influence from gravity brightening, projection, and limb darkening of the tidally distorted giant. The second panel demonstrates the added influence of reflection from the heating of the hemisphere

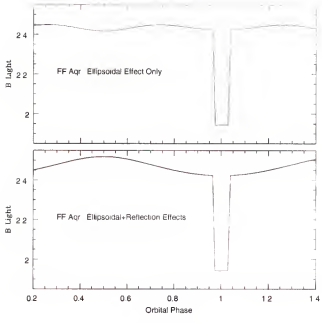

Figure 2.1: Model light curves: ellipsoidal effects (top) and ellipsoidal combined with reflection effects (bottom).

facing its hot companion. The flux in the observer's direction for a surface element is given by,

$$\Delta F_\lambda = r^2 sin\theta \ cos\gamma \ GDRI \ \Delta\theta\Delta\phi/cos\beta.$$

The angle between the line of sight and the surface normal is γ. The mean emergent polar intensity which produces the 4π steradian luminosity of the star is indicated by I. The angle between the surface normal and the radius from the center is β. G is the monochromatic gravity brightening factor. It is computed by first finding the ratio of local to polar bolometric flux,

$$\frac{F_{local}}{F_{pole}} = (\nabla\Omega)^g,$$

where ∇ Ω is normalized to the pole. The exponent g should be 1.0 for radiative envelopes, but is set to 0.3 since we are dealing with convective envelopes (Lucy 1967). Stefan's law then gives the local temperature by,

$$T_{local} = T_{pole}(\frac{F_{local}}{F_{pole}})^{0.25},$$

where G is then the ratio of the local monochromatic normal emergent intensity to that at the pole as given by Planck's law or a stellar atmosphere program. Limb darkening (D) is computed by the logarithmic law of the form,

$$D = \frac{I}{I_0} = 1 - x + xcos\gamma - ycos\gamma(ln\ cos\gamma),$$

where coefficients are tabulated by Van Hamme (1993). The reflection effect (R) is the ratio of the local monochromatic surface brightness of the affected area to the brightness in the absence of reflection. Brightness can be calculated by local temperatures (Wilson 1990). Stefan's law is used to find a new temperature of the illuminated region by considering the balance between the local bolometric flux and the bolometric energy incident from the other component.

Computations of the radial velocities utilize some of the same information generated for the light curves. Velocities for each surface element (v) are computed. Since the visible disk may show an uneven brightness due to ellipsoidal effects or spots, a flux weighted mean of the disk's velocity (ΔV) relative to a component's center of mass is computed by,

$$\Delta V = \frac{\int vFd\sigma}{\int Fd\sigma},$$

where dσ is an element of surface area. The observed radial velocity of the star, ignoring the systemic velocity (V_γ), is then,

$$V = V_c + \Delta V,$$

where V_c is the center-of-mass velocity of the star. A detailed description of the method used in the program for computing these velocities, specifically as to how it applies to tidally distorted stars, is made by Wilson and Sofia (1976).

Spectral profile modeling is a relatively new feature of the WD program. It was initially added by Dr. Robert Wilson around 1996. The routine creates profiles with a specified central wavelength for regions that are defined in the same way

as spots (longitude, co-latitude, and angular radius). The profiles are generated by rectangular elements arising from grid points that make up the stellar surface. They are binned in wavelength as they are spread out by rotational Doppler shifting. The surface elements follow solid body rotation. The profile elements are defined as emission or absorption and given a rectangular line width and intensity. The profile conforms to the given equivalent width (EW) parameter. This EW has the usual astrophysical definition. Considering an absorption line, the EW is the width in wavelength units (microns) that a profile would have if it were described by a rectangle centered on the line and bounded by the continuum and zero intensity. A more detailed description of the spectral profile model will be published in a paper currently under preparation.

Photometric data are first fit with a model light curve, starting with expected stellar attributes. Dark spots are added to these models to better fit the wave distortions. The resulting parameters are then combined with radial velocity information obtained from the spectroscopy and passed on to the differential corrections (DC) routine of the WD program. The corrections refine the parameters of the binary including orbital period, initial epoch, orbital separation, gravitational potential, and spot characteristics (location, size, and temperature).

The DC routine involves an iterative process to adjust parameters via least squares fits of multicolor light curves and one or two velocity curves. The general form of the equation of condition is

$$f_{obs} - f_{comp} = \frac{\partial f}{\partial p_1}\Delta p_1 + \frac{\partial f}{\partial p_2}\Delta p_2 + \cdots + \frac{\partial f}{\partial p_n}\Delta p_n,$$

where the functions (f) are relative fluxes (*light*) or velocities and p_1, p_2,..., p_n are parameters. The terms $\Delta p_1, \Delta p_2$, *etc.* are corrections to the parameter values from the previous iteration; therefore, each iteration has a model curve computed as

$f(p_1, p_2, \ldots, p_n, time)$. Most of the derivatives $\partial f/\partial p_n$ are found by differencing,

$$\frac{\partial f}{\partial p_n} = \frac{f(p_n + \frac{1}{2}\delta p_n) - f(p_n - \frac{1}{2}\delta p_n)}{\delta p_n},$$

although a few derivatives can be found analytically.

The mass ratios and temperatures were assumed from the literature. The values were based on mass functions, spectroscopic solutions, and expected mass ranges for a star's spectral type and luminosity class. The literature also supplied starting values for inclinations that fit light curves and were consistent with the mass, temperature, and size of the stars. Inclinations can be refined for systems with a well established mass ratio and a known absolute stellar radius. Velocities for both stars are needed for accurate mass ratios. The known rotation period requires a specific size to rotationally Doppler broaden a model profile to fit an observed photospheric line. A change of a few degrees in the inclination does not greatly affect the rotational velocity but it does impact the eclipse geometry.

Careful attention was paid to these parameters so that radial velocity and light curve models fit the data, and that they complied with an appropriate ephemeris, which would be used in generating the Hα profiles emitted from the irradiated region on the secondary. The fluorescing region is defined in the model to originate at the sub-stellar point on the cool star and conform to an angular radius described by the geometry. The profile model allows us to put a photospheric absorption line on the star as a whole. The line strength is calibrated with an equivalent width parameter that sufficiently fits the observed profile from spectra taken during mid eclipse when none of the fluorescing region is expected to be visible. A source of emission is similarly made to fit the observed profile of emission, which is placed on the surface of the secondary at the sub-stellar point to mimic a chromospheric line. Ideally this emission will be calibrated at inferior conjunction of the hot star when the illuminated region is in full view. The only line-broadening effect in the profile generation is that of rotational Doppler broadening. A simple demonstration of the

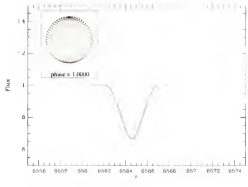

Figure 2.2: The Hα profile model of the back side of the star (eclipse).

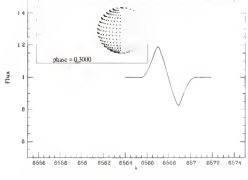

Figure 2.3: The Hα profile model showing the fluorescing region rotating into view (phase=0.30).

model can be seen in Figures 2.2-2.4. The stellar images in the figures were made with Binary Maker (Bradstreet 1993).

2.2 The Candidate Systems

The best candidates for this study are the well known binary V471 Tau and the somewhat analogous FF Aqr. Both are eclipsing binaries with phase dependent emissions that are expected to be from fluorescence. Their circular orbits and rotational synchronization of the secondary simplify the geometry of the illuminated region. The binaries are detached and there are no complications from rapid mass transfer or accretion disks. Both binaries are relatively bright ($V \approx 9^m.0$) and therefore are accessible to moderate sized ground based telescopes and require short exposure times.

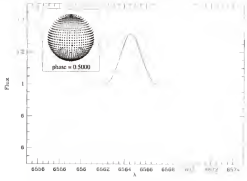

Figure 2.4: The Hα profile model with fluorescing region in full view (phase=0.50).

V471 Tau has become one of the best known and thoroughly studied star systems since its discovery as an eclipsing binary (Nelson & Young 1970). It is composed of a white dwarf primary and a K2V red dwarf secondary in a close 12.5 hour orbit. The mass ratio is very near unity and the total mass of the system $\approx 1.6 M_\odot$. These values were found by supplementing optical radial velocities with velocity measurements of the white dwarf's Lα line observed at the quadratures (Schaefer *et al.* 1995). The red dwarf has a radius $\approx 0.8 R_\odot$ while the white dwarf is considerably smaller at $\approx 0.01 R_\odot$. Its physical characteristics, evolutionary status, and membership in the Hyades cluster have provided solid evidence about the structure of white dwarfs, the role of tides in stellar systems, and the results of common-envelope evolution (Bois *et al.* 1988; Skillman and Patterson 1988; Martín *et al.* 1997; Barstow *et al.* 1997). Continued orbit shrinkage by mechanisms of gravitational radiation and magnetic wind braking will eventually cause the red dwarf to overfill its Roche lobe and begin mass transfer to its white dwarf companion. Its current state places the system into the class of pre-cataclysmic variables (pre-CV).

FF Aqr serves as a close analog to V471 Tau in terms of orbital and fluorescent characteristics while offering different types of stars. Its eclipsing and chromospherically active nature was discovered by a photometric and spectroscopic campaign (Dworetsky *et al.* 1977). Its primary is a sdOB (sub-dwarf) and it has a G8III (red giant) secondary component. The orbital period is much longer than V471 Tau's at

about 9.2 days. Etzel *et al.* (1988) found the masses and radii as $2.0M_\odot$ and $5.7R_\odot$ for the giant star and $0.5M_\odot$ and $0.14R_\odot$ for the subdwarf. Model light curves made by Dorren *et al.* (1983) show FF Aqr to have dark spots that cover ≈40% of the giant's surface and are ≈800K cooler than the surrounding photosphere. Spectroscopy of the Hα region by Marilli *et al.* (1995) in the 1990 and 1991 seasons clearly shows phase dependence.

CHAPTER 3
THE DATA

3.1 Our Observations

We made photometric and spectroscopic observations at Kitt Peak National Observatory (KPNO) on the nights of October 29 through November 9, 1998. Our primary program stars were V471 Tau and FF Aqr. I obtained spectra using the Coudé Feed 0.9m telescope. It was for this telescope that KPNO funded my observing run. The Southeastern Association for Research in Astronomy (SARA) granted us time on their 0.9m telescope as first-time guest observers. The SARA telescope is also located at the KPNO facility and was operated by Dr. Robert Wilson. This observing arrangement enabled us to get simultaneous photometric and spectroscopic coverage of our objects.

Most nights were fairly clear with only a few nights partially ruined by clouds, high winds, humidity, or fog. Observations of V471 Tau on the night of November 5 were rendered worthless due to the proximity of the full moon. FF Aqr was visible for the first few hours after sunset and was our first target while we waited for V471 Tau to rise.

3.2 Photometry

The SARA telescope was equipped with a CCD camera with a 9 arc minute square field of view. We double binned the pixels to get 1024 X 1024 images. This resolution (0.5 arc seconds per pixel) sufficiently sampled the large out-of-focus stellar images and avoided overexposure. The binning also reduced the data size for storage purposes. Each target's comparison star fit within the field so that program and comparison stars were imaged in a single exposure. Standard Johnson B, V, R,

and I filters were used. Three exposures were taken with each filter before cycling on to the next one. Exposure times varied with the filter and ranged from a typical 7 seconds in I to 40 seconds in B. The frames were processed with the Image Reduction and Analysis Facility software (IRAF), which is made available by the National Optical Astronomy Observatories. The standard IRAF task *DAOPHOT* for aperture photometry was used. The seeing was rarely one arc second quality and many of the images were out of focus so a large aperture with a radius of 15 pixels was used for all of the frames. There were no problems with stellar crowding so a 5 pixel wide annulus around this aperture was used to sample the background sky. Differential magnitudes between the comparison and program stars were produced for each frame.

Some technical difficulties arose with our inaugural, guest usage of the SARA telescope that degraded or even invalidated some of the photometric data. The dome did not rotate automatically with the telescope and had to be adjusted throughout the night by the observer. Several dozen sets of observations were thrown out because the dome started to cut off the comparison star in the field, which would artificially brighten the target star. There were no dimmer switches on the lights used to illuminate the screen on the dome for flat field imaging and the screen was torn. Exposures shorter than a few seconds were ruled out because of shutter problems, so an alternative flat field strategy was used. Some twilight sky flats were taken, but the most useful flats came from sky images during a completely fogged-out evening. These "fog" flats became the standard flats by which most of the data were reduced. Anomalous data were thrown out if the observing log indicated any technical or atmospheric problems. The instrumental magnitudes of the comparison stars were plotted against airmass to evaluate and reject abnormal data that were due to the presence of clouds or obstruction by the dome. Table 3.1 lists the total number of valid observations made in each filter for both stars.

Table 3.1: Photometric coverage.

	Number of observations	
Filter	V471 Tau	FF Aqr
B	877	159
V	851	155
R	799	161
I	644	169

Table 3.2: Radial velocity lines.

Element	Wavelength Å
Fe	6400.0
Fe	6408.0
Fe	6411.7
Fe	6546.3
Fe	6625.0
Fe	6663.5
Ca	6439.1
Ca	6450.1
Ca	6462.7
Ni	6643.6

3.3 Spectroscopy

The Coudé Feed telescope was equipped with the F3KB CCD camera, grating A, and the long collimator. Exposures of 30-45 minutes had typical S/N$\sim$70, dispersion of 0.12 Å/pix, and covered $\sim$300 Å while centered near 6525 Å. A Th-Ar comparison lamp was imaged at the beginning, middle, and end of each night for wavelength calibration. The spectra were reduced with standard IRAF techniques and normalized to the continuum level. The 1d spectra were converted to text files so comparisons with models could be made. The spectra were Doppler shifted to be made heliocentric. The remaining shifts were then due only to the orbital motions of the stars and the systemic velocity relative to the Sun.

Radial velocities were measured with IRAF's *rv* package. Table 3.2 shows the photospheric lines used in determining radial velocities for the secondaries. The flux bisection method (IRAF's *center1d* task) for finding the line centers was used, as the

gaussian profile fitting algorithm does not work well with distorted profiles. Each spectrum's velocity was determined with approximately 10 lines.

CHAPTER 4
THE ANALYSIS

4.1 FF Aqr

The analysis of FF Aqr is hampered by several factors. FF Aqr is clearly rife with activity that can be seen in both our photometry and spectra. Our observations only cover 1.2 orbits, therefore, cycle-to-cycle variations are not detected. The orbit period does seem to be longer than originally published by Dworetsky *et al.* (1977) since we expected to cover the eclipse but did not. The eclipse would have given excellent timing information and enabled us to refine the ephemeris. The eclipse width and depth would have given tighter constraints on parameters such as stellar size, separation, and temperature. A significant gap in the data was the lack of color coverage at $\phi \approx 0.5$. We obtained only B data at the phase where a reflection bump is seen. The amplitude of reflection is unknown without measures in other bands and is further complicated by dark spots, whose parameters (temperature, size, and position) thereby become more uncertain. Additionally there is the question of the extent of ellipsoidal variation due to the tidal distortion of the red giant, which primarily depends on mass ratio, stellar size, and orbital separation. We are dealing with a single-lined spectroscopic binary since no lines of the sub-dwarf have been identified; its assumed mass is typical for its spectral and luminosity type (Dworetsky *et al.*). The light curve wave forms are modified by ellipsoidal variation so as to compromise spot modeling.

Our initial concern was the ephemeris so that we could correctly follow the phase dependence of the Hα line profile. Furthermore, knowledge of how the orbit period has changed could give us evolutionary insight linked to the mechanisms

responsible for other observations. The influence of spots on the light curves and the lack of eclipse coverage prevents us from using our photometry to refine the ephemeris. However, radial velocities from our spectra are useful. The differential correction routine (DC) in the WD program was used with our velocity data together with velocities from Marilli *et al.* (1995), and results checked for consistency with the discovery U photometry (Dworetsky *et al.*), which does include a well defined eclipse. This collection of data provided timing information for three epochs spanning ≈20 years.

Difficulties exist with the previously published data. The data of Marilli *et al.* are listed as observed velocities (not Heliocentric) and had to be obtained from A. Frasca via personal communication. They cover 1990, 1991 and 1994 observing seasons and have standard deviations ≈10km/s. Their data did not thoroughly cover any given cycle. The photometry of Dworetsky *et al.* is only presented graphically. I extracted those data point by point from a scan of the plot and scaled it in pixel space. The measurements were converted from phase to time with the ephemeris in that publication. The data spanned two observing seasons and had many overlapping points, which made extraction difficult. It is unfortunate that the authors have not made the data available.

Iterations with DC were made simultaneously on our velocity data, the velocities obtained from A. Frasca, and the U photometry. The initial epoch (T_0=2442752.9577) and orbit period (P=9.207755 days) from the existing ephemeris were used as a starting point. A new ephemeris was found with iterations that left the semi-major axis (a), P, systemic velocity (V_γ), and T_0, as free parameters. The potential of the giant star was also allowed to vary so that the eclipse width would be fit. The stellar radii are not uniquely determined by this approach since they depend on the assumed inclination, mass ratio, and the resulting size of the orbit. Further iterations refined the values and included the free parameter dP/dt. The standard deviation

Table 4.1: FF Aqr parameter solutions.

Parameter	Value
T_0 (HJD_0)	42752.9544±0.0003
P	9.20801±0.00004 days
$\frac{dP}{dt}$	–
e	0.00
q	4.00
a	21.7±0.5 $R_\odot$
V_γ	23.0±0.4 km/s
i	81°
T_1	35000 K
T_2	4758 K
M_1	0.32 $M_\odot$
M_2	1.27 $M_\odot$
R_1	0.1 $R_\odot$
R_2	5.4 $R_\odot$

was more than twice the determined value of dP/dt. The final solution is based on a constant period; however, there is an increased value for the period over the original ephemeris. The results in Table 4.1 were used to make model velocity curves that fit our data (Figure 4.1). Light curve models were compared to the U photometry of Dworetsky *et al.* (Figure 4.2) to verify the eclipse geometry. A large spot near the pole was needed to fit this light curve but its existence is doubtful because of the span of the observations. Spots would have significantly migrated, waxed, and waned during the 2 seasons that the data covered. The comparison is primarily for fitting the eclipse. An inclination of 81°, a mass ratio of 4.0, T_1=35,000K, and T_2=4,758K were all assumed.

We fit our photometric data with model light curves using the parameters in Table 4.2. Dark spots were needed on the red giant for the modeled curves to fit the data. Cool circular spots were added one at a time to the red giant, with typical temperature factors (temperature factor=$\frac{T_{spot}}{T_{photosphere}}$) of about 0.80. The spot parameters were refined with DC. The resulting parameters for 5 spots are in Table 4.2. Graphic models covering key phases of the orbit show the spot coverage and

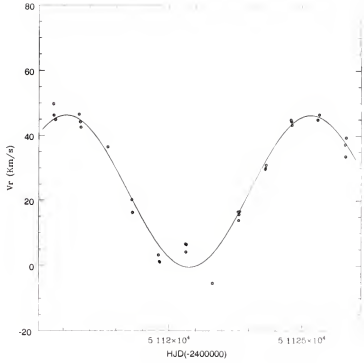

Figure 4.1: The model radial velocity curve (solid line) and our observed velocities (points).

Table 4.2: FF Aqr spot solutions.

Parameters in Radians; Temp. Factor=$\frac{T_{spot}}{T_{photosphere}}$				
Spot	Co-Latitude$\pm\sigma$	Longitude$\pm\sigma$	Radius$\pm\sigma$	Temperature Factor$\pm\sigma$
Spot 1	0.16±0.17	1.54±0.09	0.34±0.10	0.80±0.04
Spot 2	0.61±0.07	4.54±0.02	0.49±0.04	0.78±0.01
Spot 3	1.92±0.28	4.40±0.03	0.34±0.08	0.75±0.04
Spot 4	1.92±0.25	1.27±0.02	0.33±0.05	0.75±0.04
Spot 5	1.57±0.25	0.00±0.02	0.23±0.02	0.78±0.04

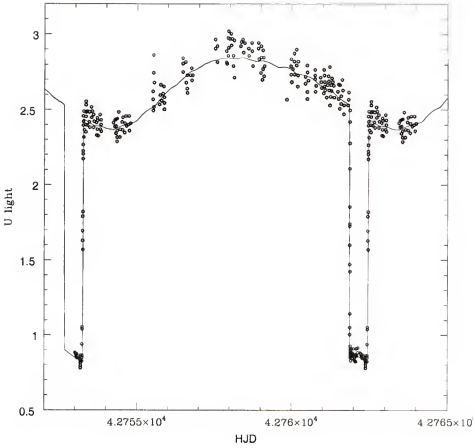

Figure 4.2: Our model light curve (solid line) and photometric measurements (points) extracted from the phase plot in the literature.

scale of the system(Figure 4.3). The four color light curve solutions can be seen in the panels of Figure 4.4. The fifth spot, at the sub-stellar point, is only needed to fit one part of the curve where the reflection bump is expected. A larger ellipsoidal effect could obviate the need for that spot. The real significance is in the other four spots that fit the data fairly well in all colors. The amount of tidal distortion of the giant does not greatly affect the spot parameters. An additional radial velocity curve was created with the spots included (Figure 4.5). Spots do have a slight effect on the curve and could account for some of the stray velocity points.

A model absorption feature was checked against an observed FeI line at 6400.0Å before modeling the Hα profiles. Since the rotation rate is locked to that of the orbit, the giant's radius had to be increased to create a broad enough profile. We adjusted the potential of the giant while keeping all other parameters fixed. A reasonably good fit was obtained with R_{giant}=7.1$R_{\odot}$ (Figure 4.6). Thus the width of the 6400.0Å line gives a handle on the absolute size of the red giant. The inclination and semi-major axis need to be adjusted for the eclipse to be fit again but the uncertainty in the mass ratio makes a unique solution impossible; therefore we did not refit the light curves and only used this new radius for fitting the profiles. We intend on doing further DC solutions for a series of mass ratios that yield consistent parameters with this newly determined radius. The results will include new values for i, a, masses, and require refinement of spot parameters.

Treating the subdwarf as a point source, there is a region of illumination on the giant's facing hemisphere with a radius of 76° as measured from the center of the giant. This area represents the part of the chromosphere where fluorescence is expected. We generated Hα profiles for all observed phases. Comparisons with the spectra at appropriate phases were necessary to calibrate the amount of photospheric absorption and chromospheric emission. The absorption profile at ϕ=0.95 was fit by inspection in order set the absorption profile for the unirradiated photosphere.

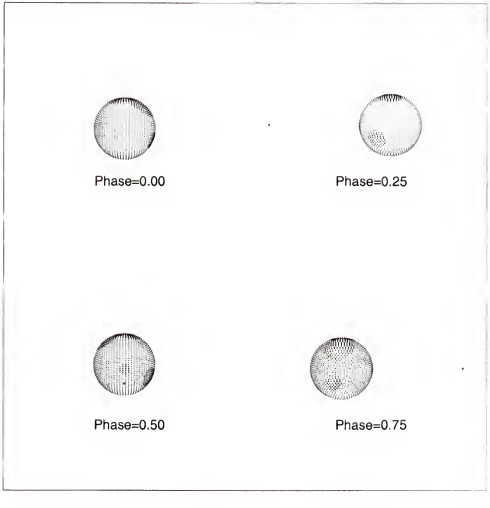

Figure 4.3: Scaled pictures of FF Aqr that show the spots used in our models. Images were made with the WD program.

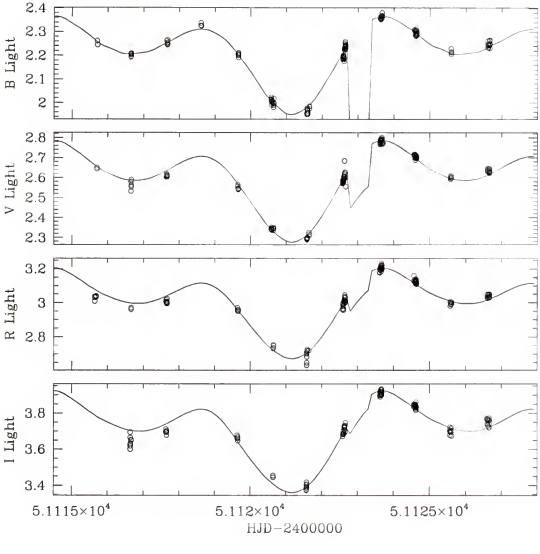

Figure 4.4: Light curve models with WD (solid line) compared with our photometry (dots) in each color observed.

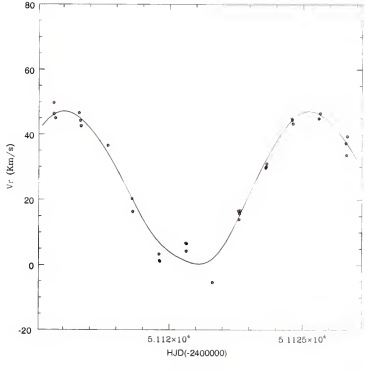

Figure 4.5: The model radial velocity curve, which includes spots (solid line) and our observed velocities (points).

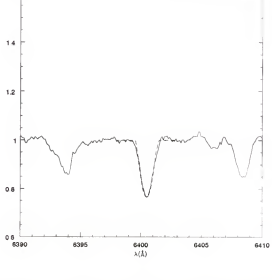

Figure 4.6: Observed spectrum of FF Aqr at ϕ=0.52 (solid line) and the modeled Fe line at 6400Å (dashed line).

Maximum emission is seen at ϕ=0.52 and the equivalent width parameter of the modeled fluorescing region was set to fit that profile. The emission profile competes with the photospheric absorption since it is formed in the chromosphere and lies on top of the absorption forming photosphere. The intermediate phases were then computed with these set parameters for both the absorbing and emitting zones.

There were no significant variations in our spectra during a given night, so only the best spectrum from each night is compared with a profile model (Figure 4.7-4.9). Although our models follow the overall trend of phase dependant emission there are striking differences. The observed profiles are almost twice as wide as the theoretical ones, there appears to be a persistent blue shifted emission, and there is a strong, broad blue shifted emission seen at ϕ=0.85.

The broad component was noted by Marilli *et al.*. Their Hα spectra show the broad emission in one of the two consecutive seasons covered. We expect the mechanism to be related to the activity of the red giant due to the profile's transient behavior. There may be a connection with spots because major spot areas are centered on the facing hemisphere near each quadrature; according to the light curve solutions. This positioning of the spots allows both regions to be seen on the approaching and receding limbs during inferior conjunction of the subdwarf. Large extended and stable coronal loops that are anchored to these spots could be forced to co-rotate with the star and give rise to the additional Doppler broadening.

Emitting sources have been investigated in the case of the fast rotating K dwarf, AB Dor (Cameron & Robinson, 1989a;1989b). They observed transient emission and absorption moving through the stellar absorption profile. Emission was seen on the blue and red wings of the profiles. Additional absorption moved across the profile with the rotation. The features were identified as extended structures that emitted when away from the limb and absorbed when projected over the facing hemisphere. The model they proposed was of neutral gas trapped in magnetic loops

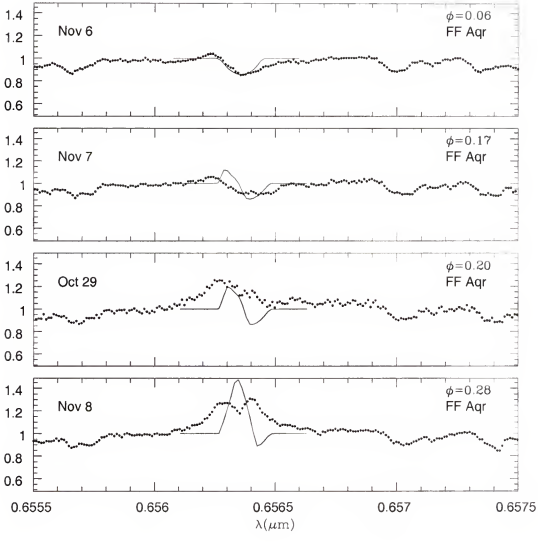

Figure 4.7: Observed spectra of FF Aqr (dots) and the modeled Hα profile (solid line) for phases 0.06-0.28.

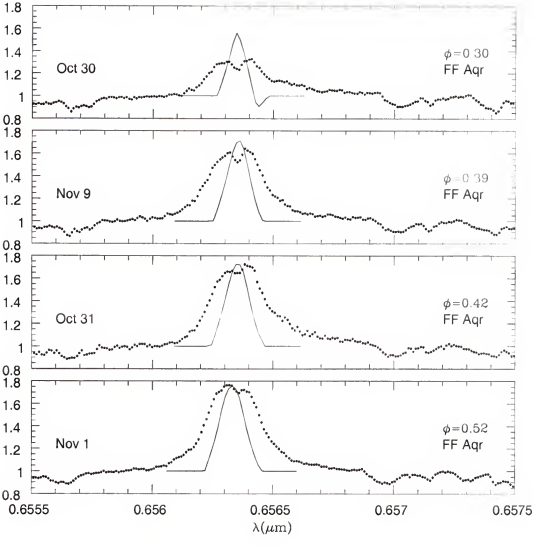

Figure 4.8: Observed spectra of FF Aqr (dots) and the modeled Hα profile (solid line) for phases 0.30-0.52.

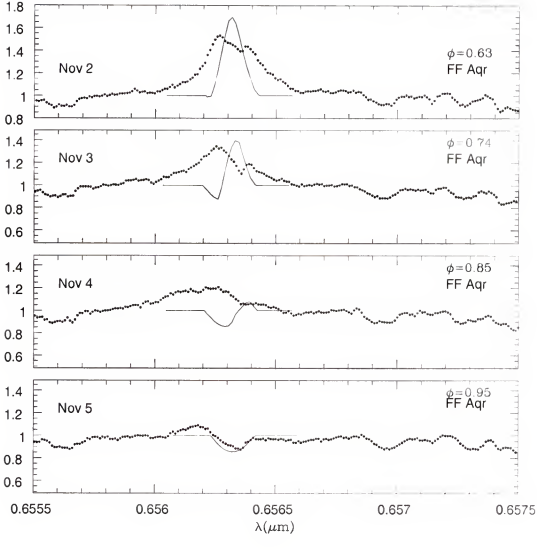

Figure 4.9: Observed spectra of FF Aqr (dots) and the modeled Hα profile (solid line) for phases 0.63-0.95.

extending several stellar radii above the surface and forced to co-rotate. These clouds persisted for a good portion of the rotation ($P_{rot} \approx 12.5$ hrs). If this model applied to FF Aqr we might expect these regions to be additional sources of fluorescence when on the hemisphere facing or nearly facing the subdwarf. If these structures are associated with polar spots then they may partially fill the absorption seen around eclipse, since they could be visible over the entire orbit. The problem with this interpretation is that we do not see a transition from blue to red shifted sides of the profiles so as to indicate that these structures are rotating. Perhaps this is due to the lifetimes of these structures being much shorter than the orbital period of FF Aqr. More phase redundancy in the observations would be needed to answer this question.

Additional support for extended regions above the surface of the red giant comes from the observations of Baliunas *et al* (1986). They observed absorption lines of species such as C II and C IV that doubled in strength during ingress and egress of the subdwarf, relative to the those seen at quadrature. They suggest that the excess absorption is caused by a geometrically extended atmosphere of the giant and that the enhancements are present to at least 1.5 stellar radii above its surface. However they believe the phenomena to be permanent since the enhancements persisted for three years.

The seemingly persistent blueward emission is more difficult to understand. It is best seen at phases not far from eclipse when it is not combined with the fluorescing chromosphere or possible extended sources. The largest example of this emission, seen at ϕ=0.85, might give some insight into the source. The emission is not then as intense as at maximum, but it is fairly wide ($\approx$3.5Å). The emission appears to diminish and narrow over the next few days, but remains on the blue side of the red star's absorption. We do not expect the source to be associated with the receding subdwarf. Again, there could be a spot connection since the two largest spot groups are almost face-on at that phase. A large eruption (flare or coronal

mass ejection) that expelled matter from the system might have emanated from these active regions. This plasma would have cooled and thinned as it moved out allowing us to see a constantly blue-shifted spectrum as it diminished in strength. The limited phase redundancy prevents us from confirming this interpretation and there is no supporting evidence in our photometry.

Mass transfer or loss in a binary can affect its orbit. Etzel(1988) states that the period has undergone a sudden increase based on a revised spectroscopic orbit and photometry from 1986 and 1987 but without any published numbers. The stars in FF Aqr should be well within their Roche lobes; therefore there should be no mass transfer by lobe overflow. A period increase due to conservative mass transfer is implausible, as it would require the low mass subdwarf to transfer mass to the giant. Mass loss from the system would cause a period increase. Although a significant dP/dt can not be found in our analysis, a period change is apparent. The possible mass loss detected in our data may be a key contributor to the period change. An upper estimate of this mass loss ($\dot{M}_2$) can be made with the formula

$$\frac{\dot{P}}{P} = -\frac{2\dot{M}_2}{M_1 + M_2},$$

if we assume an isotropic wind from the giant star (Pringle & Wade 1985). We can use a value of $\dot{P}$ based on the error in our solution that included it; therefore $\dot{P} \lesssim 10^{-7}$ may exist. Using our masses for the stars, we get $\dot{M}_2 \approx 10^{-6}\ \frac{M_\odot}{yr}$. This mass loss rate falls in the range of measured values for hot and cool luminous supergiants (Bohm-Vitense 1989). This value seems high for the giant of FF Aqr but may be enhanced due to its binary nature. A dense wind might lend support to the extended atmosphere observed by Baliunas *et al.* . It is possible that a combination or interaction of these and other mechanisms is needed to produce the complexities of the spectrum. More thorough analysis of FF Aqr must await spectral coverage that extends over at least several orbits.

4.2 V471 Tau

Our analysis of V471 Tau is more thorough than for FF Aqr. The short period (12.5 hrs) enabled us to cover about 75% of the orbit per night and recover the orbit about 0.1 phase earlier each subsequent night: therefore we obtained significant phase redundancy. There also exists almost 30 years of literature devoted to many aspects of this binary, which permit more secure assumptions regarding some parameters. With many parameters well established, we were able to focus on our data set alone.

Considerable work has focused on the orbital period. İbanoğlu (1989) discussed variations in the eclipse timings that he and others have detected (Young and Lanning 1975; Oliver *et al.* 1978; Tunca *et al.* 1979; Beavers *et al.* 1986). The period has been seen to increase and decrease. Long term effects in the O-C's have recently been investigated by Guinan and Ribas (2001). They conclude that a light-time effect of more than two minutes is caused by a tertiary component, which may be a brown dwarf with an orbital period around 30 years. It appears that a full cycle of this effect has finally been observed. They do note, however, that there are additional shorter periodicities on the order of several years with smaller amplitudes (~20 seconds). The causes of these changes are still unknown.

The third body effect was considered earlier by Bois *et al.* (1988). They gave an ephemeris with an orbital period of 0.52118334 days in the rest frame of the binary. We have adopted this value for our analysis since our coverage was short compared to any of the known period changing effects. The initial epoch(T_0) was computed with their ephemeris for the middle of our run. We assumed a mass ratio of unity as established by Schaefer *et al.* (1995) from radial velocities of the white dwarf. The temperatures were assumed as 32,400K for the white dwarf (Barstow et al. 1997) and 5,000K for the red dwarf. The eccentricity was assumed to be zero in the absence of evidence to the contrary. We originally set the inclination to 80°, the semi-major axis to $3.12R_{\odot}$, and the systemic velocity to 37km/s (Bois *et al.*). The

potentials of the stars were made to yield a white dwarf radius of nearly $0.0095R_\odot$ and a red dwarf radius of $0.75R_\odot$ (Young *et al.* 1988).

The DC routine was applied to our radial velocities to refine values of a, V_γ, and T_0. A model radial velocity curve based on our final solutions compared to our data is in figure 4.10. We then modeled an absorption profile of Hα and compared it to observed profiles seen during eclipse (phase≈0.00) when no fluorescent contribution is expected. The profile was not wide enough. The star's synchronous rotation with the orbit requires a larger stellar radius to increase the rotational Doppler broadening of the profile. A radius of nearly $0.94R_\odot$ was needed to fit the data. A similar radius was found in a Doppler imaging study of this star (Ramseyer *et al.* 1995) and is consistent with the LiI profiles fit by Martín *et al.* (1997). This is slightly oversized for a typical K dwarf. We calibrated the model's equivalent width parameter with this stellar radius to fit the profile. This absorption profile was applied to the entire star as a component of photospheric absorption.

With these stellar and orbital parameters determined, and the others assumed, we began fitting the photometric data with model light curves. The modeled eclipse width was initially too wide; probably due to the assumed inclination that may have been based on lower expected values of the secondary's size by previous authors. A lower inclination shortened the time of totality and a new value of 78° was adopted to fit the eclipse.

Although there is a noticeable amount of ellipsoidal variation in the light curve from the tidal distortion of the secondary, additional modulation is attributed to spots. Most of the light curve variation is due to spots and no significant photospheric heating by the primary has been detected (*ie.* no reflection effect). Three spots were added to the star with temperature factors of 0.80 and located near the equator. Refinements to spot locations and sizes were made with DC runs that kept the other stellar and orbital parameters fixed so as not to move the eclipse. An added difficulty

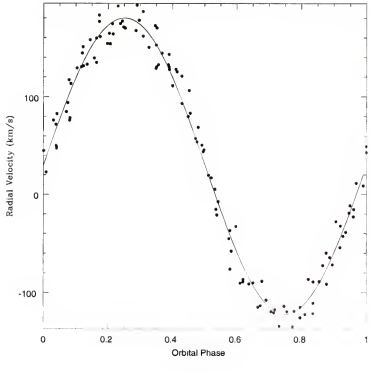

Figure 4.10: The model radial velocity curve (solid line) and our observed velocities (points).

Table 4.3: V471 Tau parameter solutions.

Parameter	Value
T_0 (HJD_0)	24451119.7270±0.0001
P	0.52118334 days
$\frac{dp}{dt}$	–
e	0.00
q	1.00
a	3.19±0.01$R_\odot$
V_γ	30.0±0.3km/s
i	78°
T_1	32400 K
T_2	5000 K
M_1	0.81 $M_\odot$
M_2	0.81 $M_\odot$
R_1	0.009 $R_\odot$
R_2	.937 $R_\odot$

Table 4.4: V471 Tau spot parameters.

Position in Radians; Temp. Factor=$\frac{T_{spot}}{T_{photosphere}}$				
Spot	Co-Latitude±σ	Longitude±σ	Radius±σ	Temperature Factor±σ
Spot 1	0.80±0.21	4.20±0.09	0.27±0.04	0.80±0.04
Spot 2	1.34±0.20	2.45±0.02	0.18±0.01	0.80±0.04
Spot 3	1.84±0.14	5.40±0.01	0.29±0.05	0.80±0.03

in solving spot parameters is that DC can only handle 2 spots at a time and there is a uniqueness problem in solving for the latitude. The final values for the stellar and orbital parameters can be seen in Table 4.3. Spot parameters are listed in Table 4.4. Standard deviations computed by DC are listed for the adjustable parameters. They were generated from a run that considers the radial velocities along with our four color photometry. The DC solutions were based on all data having equal weight.

Images of the binary showing the scale of the system and the spots are in Figure 4.11. The model light curves for all four passbands are compared to our data in Figure 4.12. The light curves are shown in phase, based on the orbital parameters in table 4.3, due to the multiple cycles that were covered. The scatter in the data is not indicative of that seen in a single night and could be attributed to the migration

of the spots over 12 days. A six month period was found for the wave migration by İbanoğlu (1989). The wave has been known to move through the light curve in the retrograde sense; requiring a super-synchronous motion of the spots as they appear earlier in phase over time. All spots were fixed in position and rotated with the star as we did not attempt to model spot motion.

Figures 4.13-4.48 show our Hα spectra of V471 Tau along with a model profile. The data are binned in intervals of 0.01 phase due to considerable redundancy. There is a telluric feature around 6564Å which must be kept in mind when looking at the spectra. Another telluric line at 6572Å that does not affect Hα can be used as a reference as to the strength of the interloping line at 6564Å. There are clear variations seen in the spectrum at almost every phase that was observed more than once. Asymmetries in the absorption and emission profile of Hα can be seen on different nights. Transient emissions, such as flares, may be the cause of the distorted profiles. The spectra seen at each conjunction show the expected behavior of deepest absorption (phase=0.00) and highest emission (phase=0.50).

The source of fluorescent emission was modeled as a circular spot with an angular radius of 76° as measured from the center of the secondary. The spot size is defined by the geometry and represents the chromosphere of the red star that is illuminated by the white dwarf. We were prevented from using the maximum emission seen at phase 0.50 for calibrating the equivalent width parameter of the profile by the following circumstance: an excess source of Hα emission is seen around phase 0.25 on the blueward side of the secondary's photospheric/chromospheric Hα profile (Figure 4.22). This excess shows on the redward side around phase 0.77 (Figure 4.40), and enhances what we see at phase 0.50; therefore a calibration at that phase would overestimate the contribution from the expected fluorescent zone.

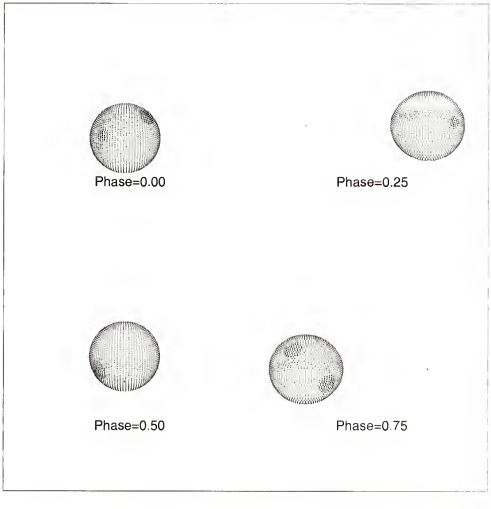

Figure 4.11: Scaled pictures of V471 Tau that show the spots used in our models. Images were made with the WD program.

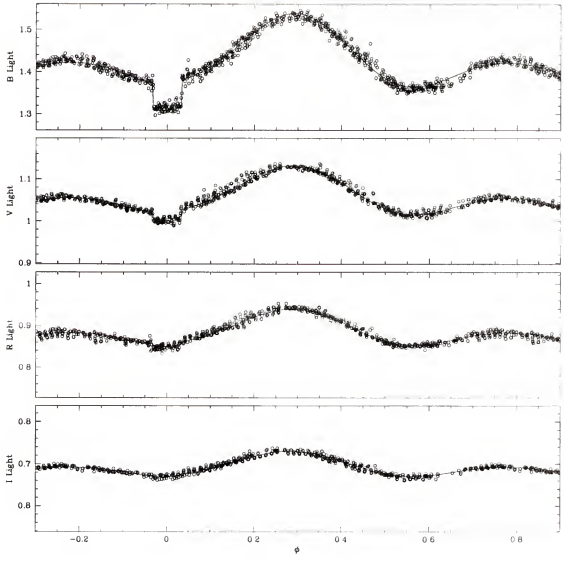

Figure 4.12: Light curve models with WD (solid line) compared with our photometry (dots) in each color observed.

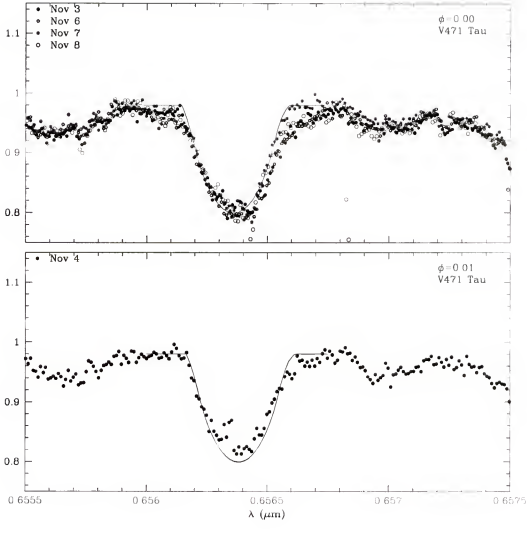

Figure 4.13: Observed spectra of V471 Tau (symbols) and the modeled Hα profile (solid line) for phases 0.00-0.01.

At phases 0.25 and 0.75 the excess is at maximum displacement from the secondary's *normal* Hα profile (approximately 4Å from line center). The width of this emission is around 3Å, so little contamination of the fluorescent region is expected at the quadratures. A calibration of the fluorescent emission was achieved with the phase 0.25 spectra (Figure 4.22). We fit the emissive bump seen on the blueward side of the normal photospheric absorption profile there. It was the only way to isolate the fluorescent zone, which is rotating into view at that time. If limb darkening is an issue with the fluorescent effect then this calibration might underestimate the emission when it is in full view at phase 0.50.

The absorbing component (photosphere) and the emitting component (chromospheric fluorescence) combine to produce the profiles modeled for each phase observed. According to our method of calibration, the fluorescent zone only fills in the absorption and barely rises above the continuum when in full view (phase=0.50). Our model at phase 0.50 might represent what Rottler *et al.* (1998) saw in their 1992 spectra. They concluded that the fluorescent component is below detection and that all previously observed emission above the continuum arises from a persistent active region at the substellar point of the secondary. This would indicate a low level of activity for the secondary during the 1992 season. Photometry taken in 1992 by Tunca *et al.* (1993) show a low level of distortion in the light curve, which means spot activity was indeed low. We begin to see a spot cycle when we consider the lack of activity in 1992, the activity in our data (1998), and the quasi-periodicity of mean brightness variations noted by (1989), which show average B and V minima during the years 1973 and 1985. This activity corresponds to a 12 year spot cycle, which is very similar to the 11 year solar cycle.

The excess emission repeatedly sweeps across the secondary's Hα region over the same range of phases. It becomes noticeable on the blue side of the secondary's Hα absorption around phase 0.1, overlaps the line at phase 0.5, and disappears on

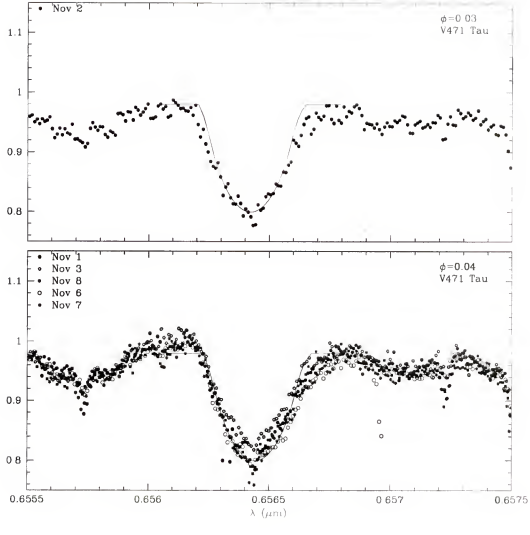

Figure 4.14: Observed spectra of V471 Tau (symbols) and the modeled Hα profile (solid line) for phases 0.03-0.04.

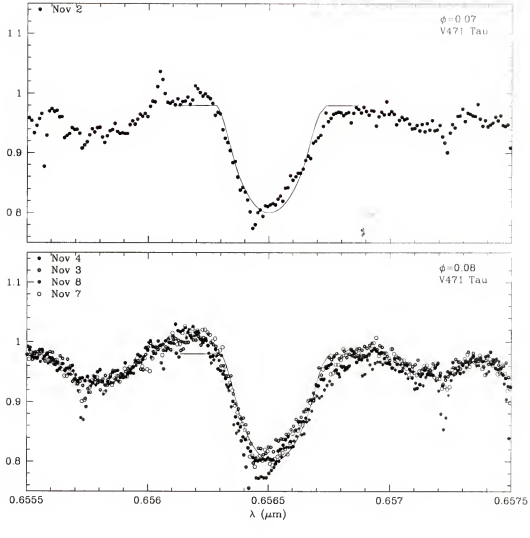

Figure 4.15: Observed spectra of V471 Tau (symbols) and the modeled Hα profile (solid line) for phases 0.07-0.08.

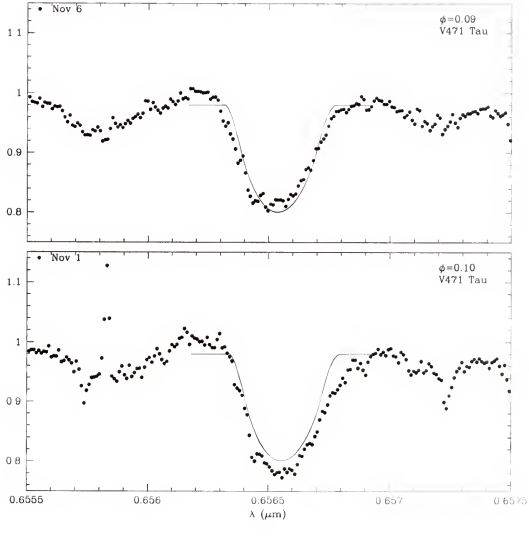

Figure 4.16: Observed spectra of V471 Tau (symbols) and the modeled Hα profile (solid line) for phases 0.09-0.10.

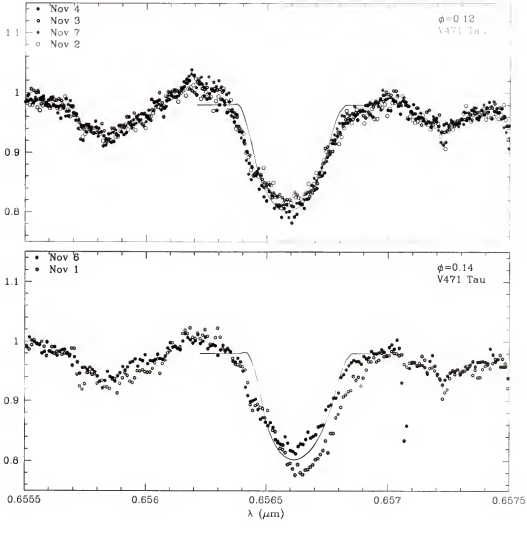

Figure 4.17: Observed spectra of V471 Tau (symbols) and the modeled Hα profile (solid line) for phases 0.12-0.14.

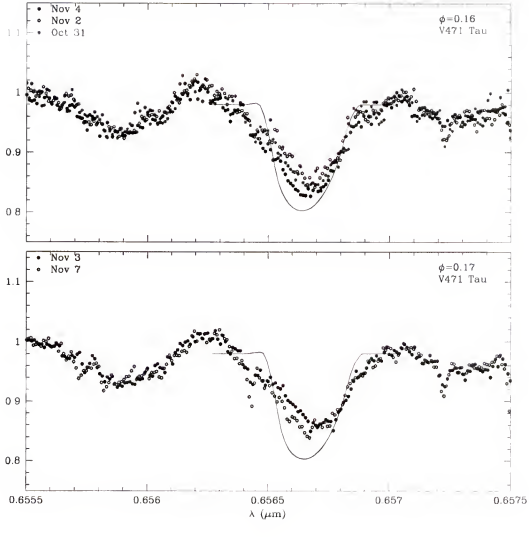

Figure 4.18: Observed spectra of V471 Tau (symbols) and the modeled Hα profile (solid line) for phases 0.16-0.17.

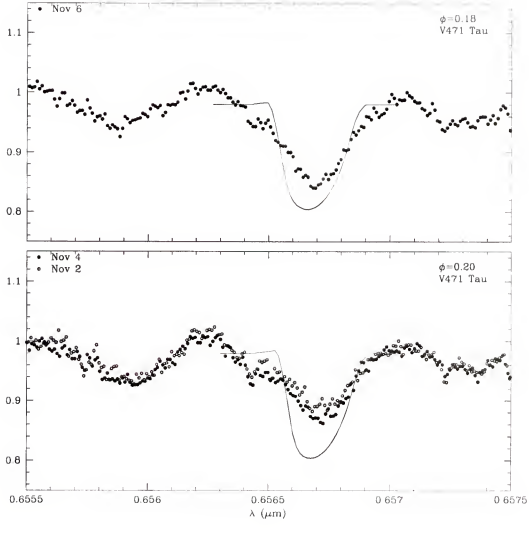

Figure 4.19: Observed spectra of V471 Tau (symbols) and the modeled Hα profile (solid line) for phases 0.18-0.20.

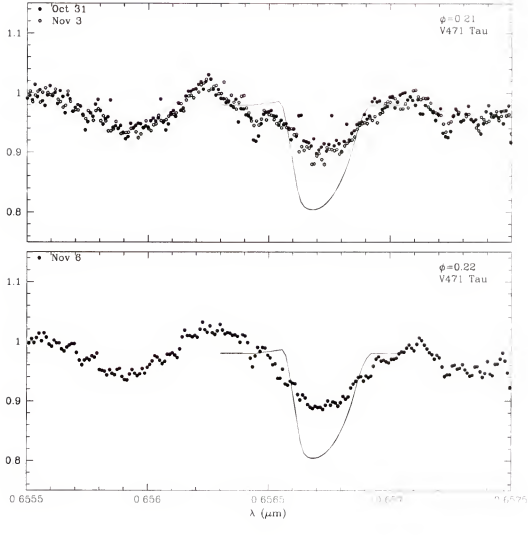

Figure 4.20: Observed spectra of V471 Tau (symbols) and the modeled Hα profile (solid line) for phases 0.21-0.22.

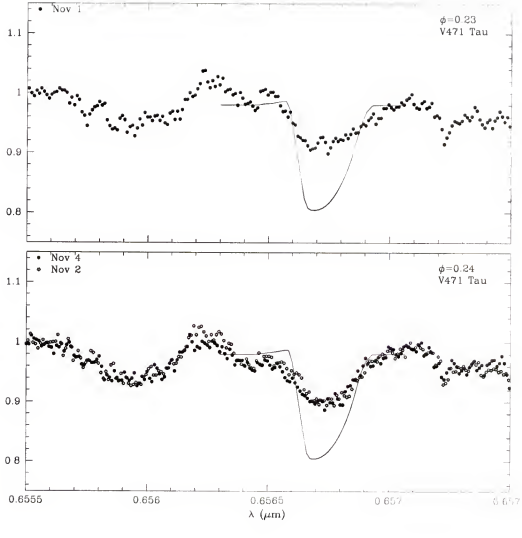

Figure 4.21: Observed spectra of V471 Tau (symbols) and the modeled Hα profile (solid line) for phases 0.23-0.24.

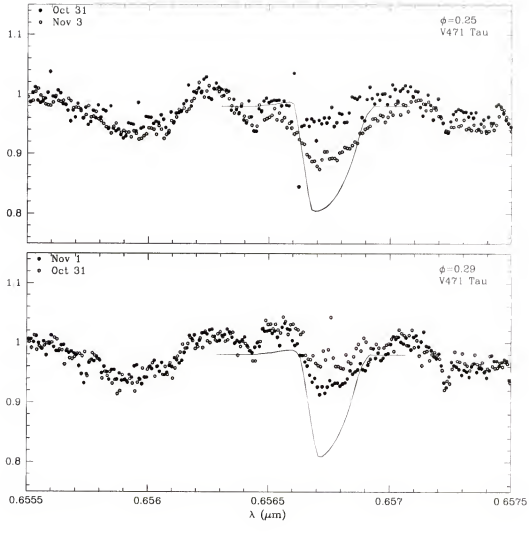

Figure 4.22: Observed spectra of V471 Tau (symbols) and the modeled Hα profile (solid line) for phases 0.25-0.29.

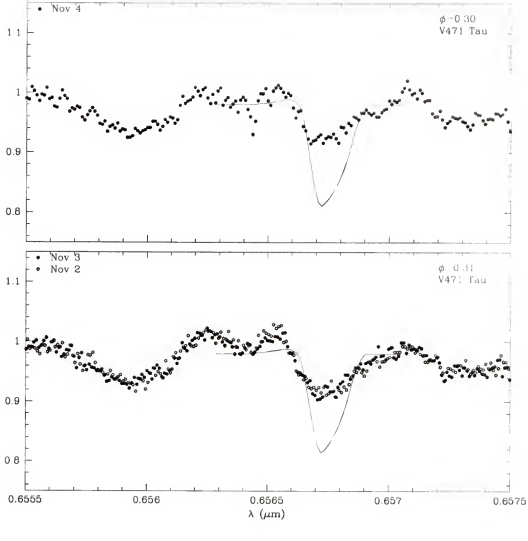

Figure 4.23: Observed spectra of V471 Tau (symbols) and the modeled Hα profile (solid line) for phases 0.30-0.31.

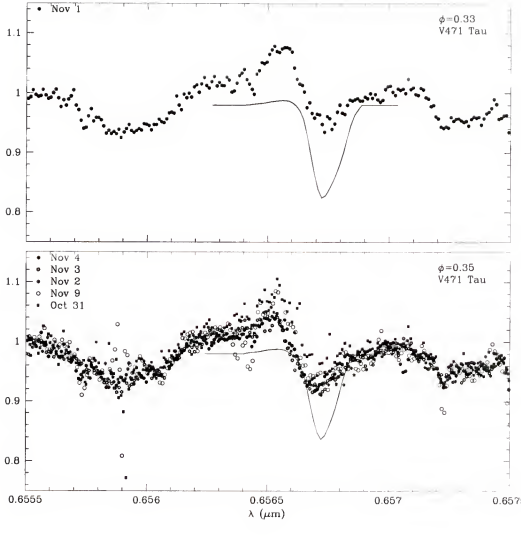

Figure 4.24: Observed spectra of V471 Tau (symbols) and the modeled Hα profile (solid line) for phases 0.33-0.35.

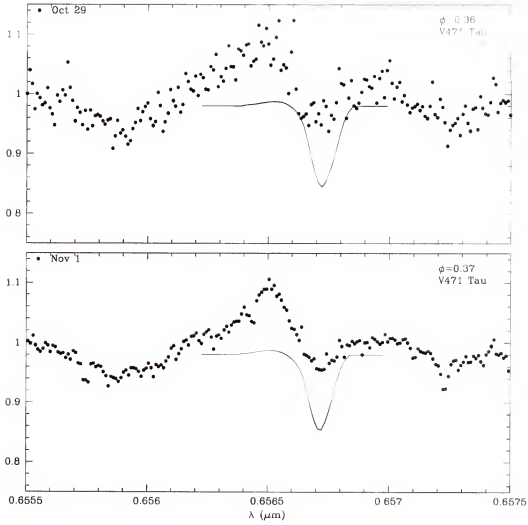

Figure 4.25: Observed spectra of V471 Tau (symbols) and the modeled Hα profile (solid line) for phases 0.36-0.37.

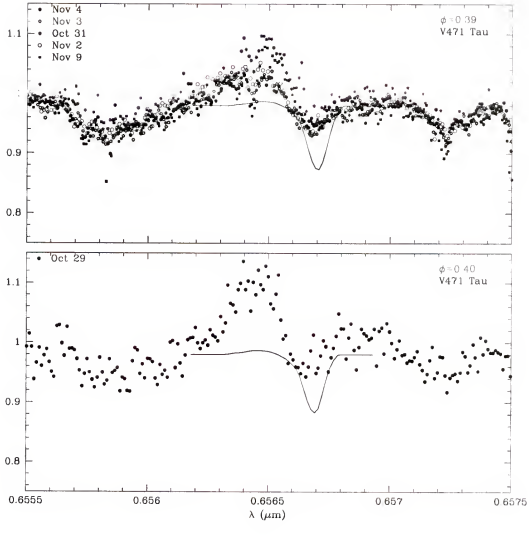

Figure 4.26: Observed spectra of V471 Tau (symbols) and the modeled Hα profile (solid line) for phases 0.39-0.40.

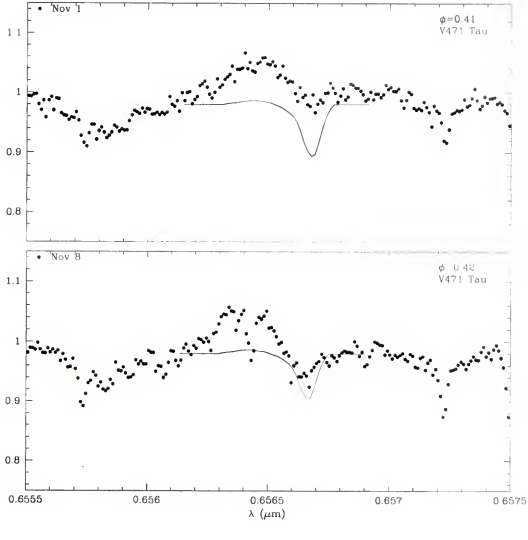

Figure 4.27: Observed spectra of V471 Tau (symbols) and the modeled Hα profile (solid line) for phases 0.41-0.42.

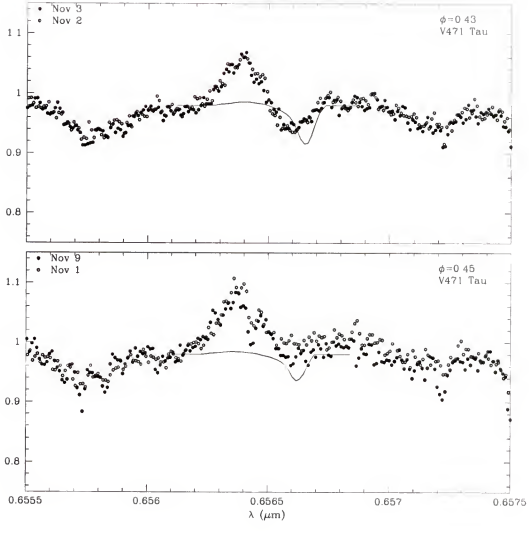

Figure 4.28: Observed spectra of V471 Tau (symbols) and the modeled Hα profile (solid line) for phases 0.43-0.45.

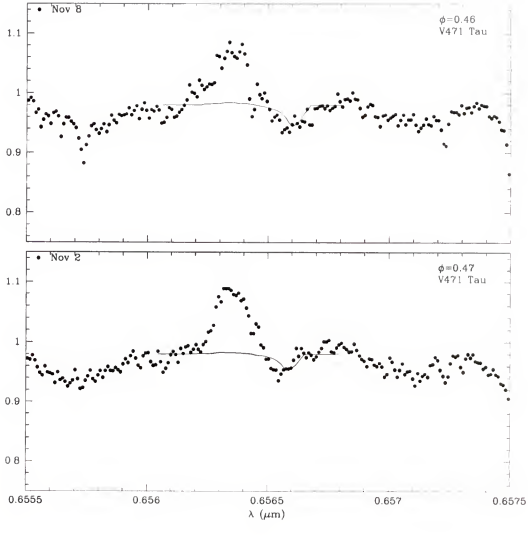

Figure 4.29: Observed spectra of V471 Tau (symbols) and the modeled Hα profile (solid line) for phases 0.46-0.47.

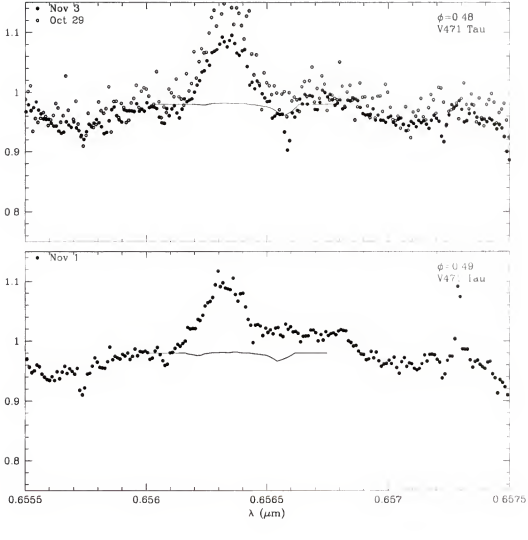

Figure 4.30: Observed spectra of V471 Tau (symbols) and the modeled Hα profile (solid line) for phases 0.48-0.49.

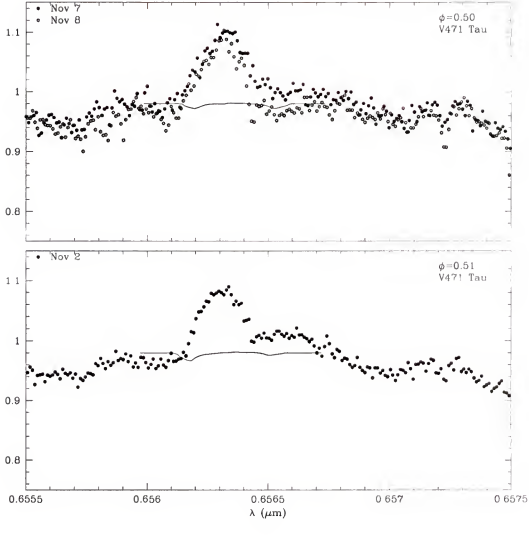

Figure 4.31: Observed spectra of V471 Tau (symbols) and the modeled Hα profile (solid line) for phases 0.50-0.51.

the blue side around phase 0.9. The phase dependence of the excess suggests that it is co-rotating with the system. The maximum displacement of the excess near the quadratures yields a velocity of 180 km/s relative to the secondary's rest frame. This velocity places it well above the surface of the secondary and close to the point between the stars if it does lie along the line of centers.

The strength and shape of the excess profile varied little from night to night. It appears that more emission was present at the beginning of our observing run and that it decreased over several days. The bottom panel of Figure 4.24, both panels in Figure 4.26, and the top panel of Figure 4.30 show that the emission was highest on the nights of October 29 and 31; thereafter, it remained rather constant.

Young *et al.* (1991) saw a similar excess of Hα near the orbital quadratures on two separate observing runs. Observations on two consecutive nights in November, 1985 (2 spectra taken near phase 0.25) and January, 1986 (two spectra taken near phase 0.75) contain a source of emission that is shifted by nearly 180km/s in the same sense that our data show. The initial detection of this excess emission took place on the second night in November. They suggest a connection to a flare event that occurred on the previous night. The later data in January shows a similar excess on the red side of the Hα profile along with an accompanying weaker source on the blue side. They interpret the dual appearance of the excess as evidence of a ring or disk around the K dwarf. The weaker component is supposedly ionized by coronal X-radiation of the secondary itself. Although a persistent weak source opposite our detected excess is not seen, we do not know the level of the coronal X-rays and, if low, the weak source could be undetectable. The higher level of emission seen on the first few nights of our data may be consistent with an eruptive event as the source.

The non-interacting multiple star AB Dor (Guirado *et al.* 1997) provides us with the best comparison to the secondary in V471 Tau. The primary in AB Dor is a rapidly rotating K dwarf with a similar rotation rate to that of the secondary in

V471 Tau. Its rapid rotation is due to its young age rather than being tidally induced by an orbiting companion. It exhibits the characteristics of chromospherically active stars (spots, flares, X-rays, etc.). AB Dor's companions are low mass objects that are in wide orbits; therefore, no gravitational interaction or radiative effects from a nearby star influence the activity seen on the K dwarf.

Co-rotating prominence formations have been detected around AB Dor via the Balmer lines (Donati *et al.* 1999). These clouds persisted for 2-4 rotations with velocities that place them 2.7 to 4.7 stellar radii away from the stellar rotation axis. These clouds produce transient absorption features in the Hα profile as they cross the stellar disk. It is believed that neutral hydrogen is forced to co-rotate at a distance above the stellar surface and held there by magnetic fields.

Similar structures appear to exist on the secondary of V471 Tau providing additional emission as they fluoresce in the presence of the white dwarf's UV radiation field. The magnetic field confinement of this gas explains the phase dependence of the excess emission observed in our data by forcing co-rotation. It also explains the high velocity, which places the gas well above the surface where it is supported by the balance of centrifugal and gravitational forces. The lifetimes of the prominences in AB Dor correspond to the first few nights that the observed excess in V471 Tau was strong.

There may also be a spot connection with the excess since a large spot is centered near phase 0.6 (Figure 4.11); close to 0.5 phase at which the excess appears centered on the profile. This spot may be the foundation for the magnetic field forming the prominence. A correlation between spots and extended structures on V471 Tau was found by Guinan *et al.* (1986). They used photometry to locate the spotted regions on the secondary and found that they were located near the limbs when contemporaneous spectroscopy showed UV absorption during eclipse ingress and egress. Absorption lines of CII, CIII, CIV, OI, SiIII, SiII, and SiIV were seen

superimposed on the white dwarf spectrum. The lines are formed as light from the white dwarf is intercepted by cool gas that is 300,000-400,000km above the surface of the secondary. Line strength analysis revealed a temperature around 10^5K and an electron density of 10^{10}-10^{11} cm^{-3}.

The profile asymmetries and distortions in V471 Tau could be attributed to heating, ionization, and the gravitational influence of the white dwarf. Accretion onto the white dwarf would prevent the structures from getting much larger than several stellar radii. The white dwarf in V471 Tau is known to be a polar accretor from its 555 second X-ray modulation, which is explained by a magnetic rotator model (Clemens *et al.* 1992). The angular momentum losses and possible mass transfer scenarios, which would occur via this mechanism, can contribute to the small amplitude variations of the orbital period noted by Guinan and Ribas.

Fitting model absorption profiles to spectra taken during eclipse provides a template for detecting emissions from other mechanisms. This is true for both FF Aqr and V471 Tau. We may not be able to perfectly model the chromospheric fluorescence at this time but the template reveals the combined activities that are present on the stars. While neither star may ever show an immaculate hemisphere, because of continuous activity, the observed absorption during eclipse would serve as a typical profile that can be applied to the whole star. Continued monitoring of these stars will provide more information about their activity cycles so that a quiescent period might be observed and the chromospheric fluorescence calibrated.

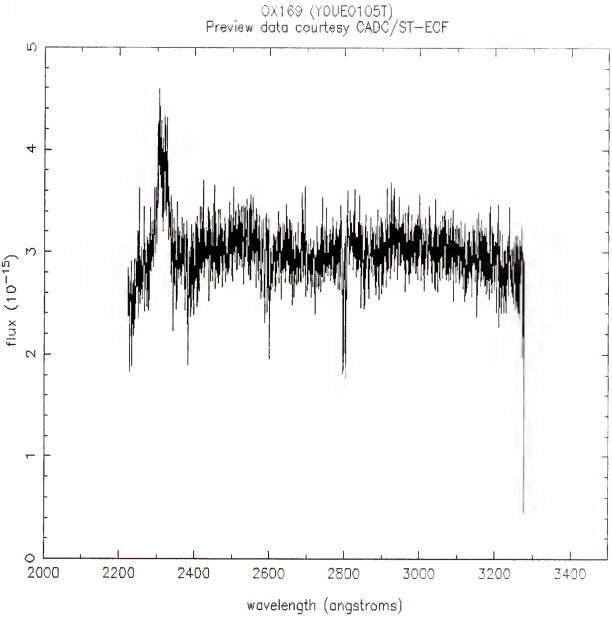
OX169 (Y0UE0105T)
Preview data courtesy CADC/ST-ECF
flux (10^{-15})
0
1
2
3
4
5
2000
2200
2400
2600
2800
3000
3200
3400
wavelength (angstroms)

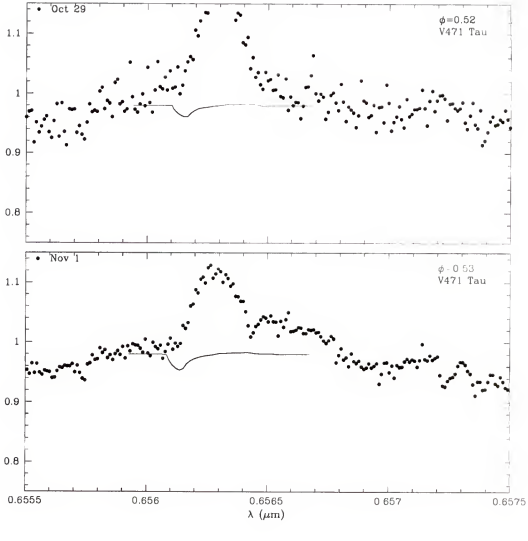

Figure 4.32: Observed spectra of V471 Tau (symbols) and the modeled Hα profile (solid line) for phases 0.52-0.53.

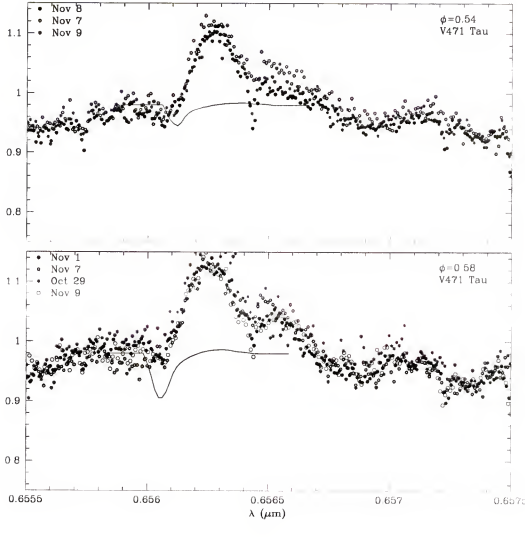

Figure 4.33: Observed spectra of V471 Tau (symbols) and the modeled Hα profile (solid line) for phases 0.54-0.58.

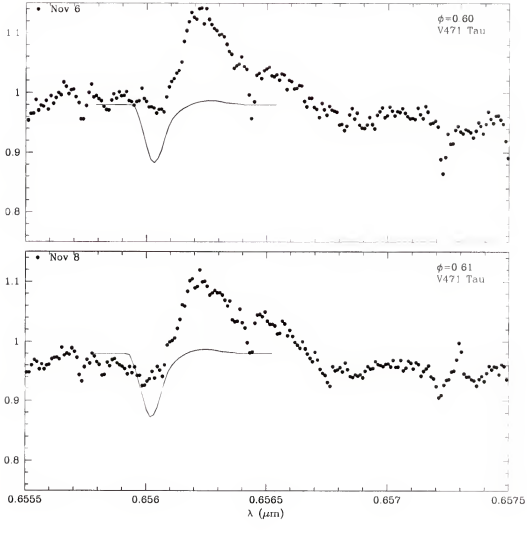

Figure 4.34: Observed spectra of V471 Tau (symbols) and the modeled Hα profile (solid line) for phases 0.60-0.61.

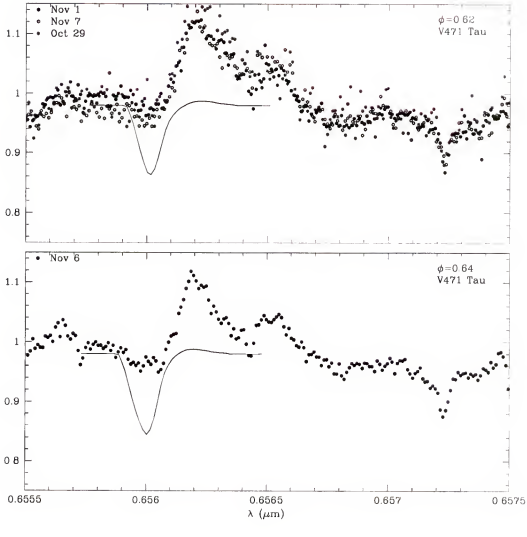

Figure 4.35: Observed spectra of V471 Tau (symbols) and the modeled Hα profile (solid line) for phases 0.62-0.64.

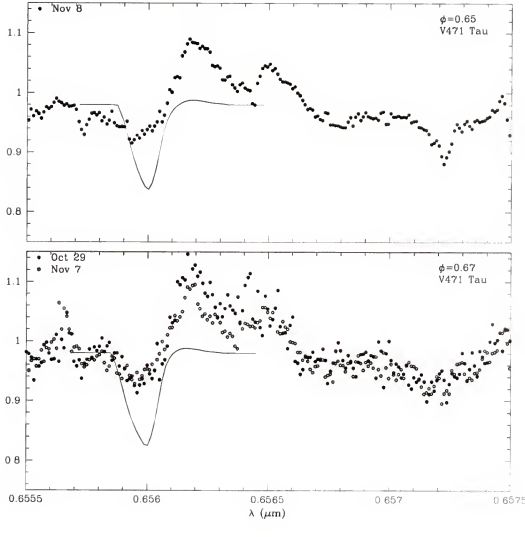

Figure 4.36: Observed spectra of V471 Tau (symbols) and the modeled Hα profile (solid line) for phases 0.65-0.67.

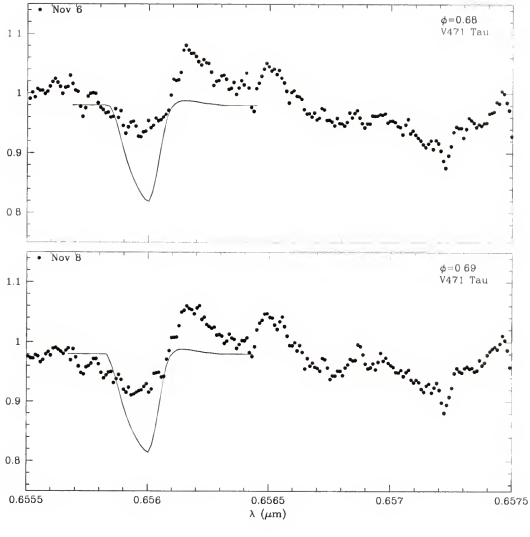

Figure 4.37: Observed spectra of V471 Tau (symbols) and the modeled Hα profile (solid line) for phases 0.68-0.69.

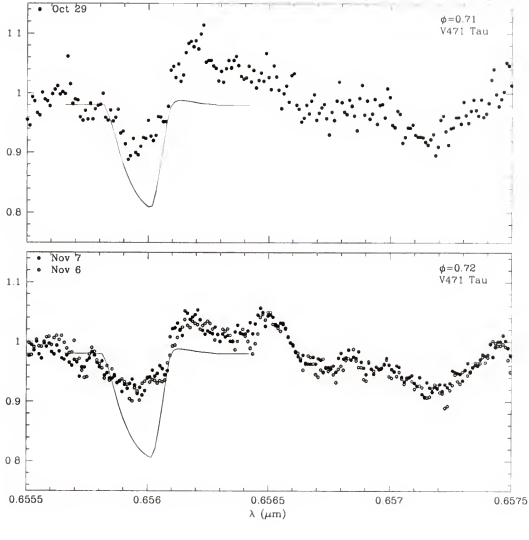

Figure 4.38: Observed spectra of V471 Tau (symbols) and the modeled Hα profile (solid line) for phases 0.71-0.72.

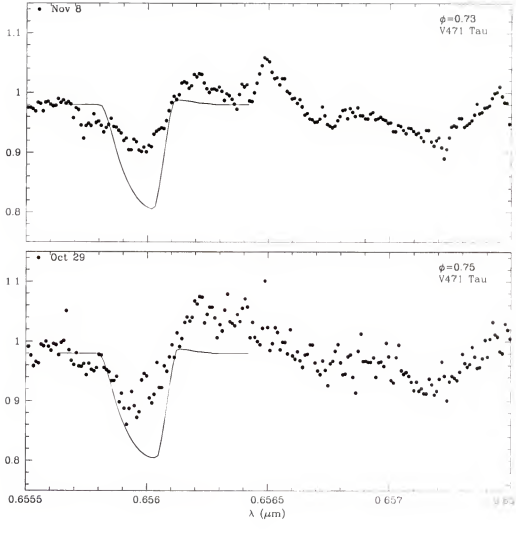

Figure 4.39: Observed spectra of V471 Tau (symbols) and the modeled Hα profile (solid line) for phases 0.73-0.75.

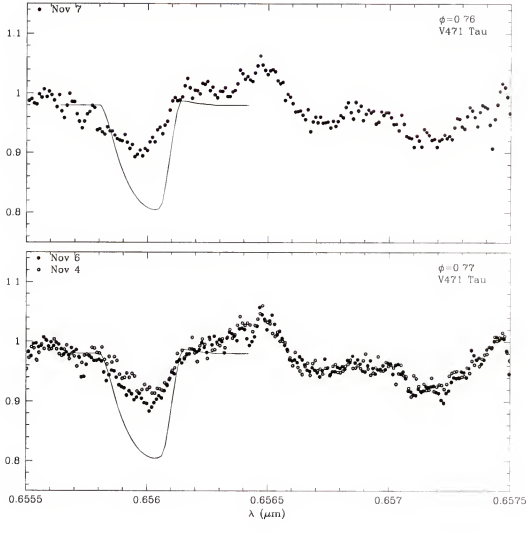

Figure 4.40: Observed spectra of V471 Tau (symbols) and the modeled Hα profile (solid line) for phases 0.76-0.77.

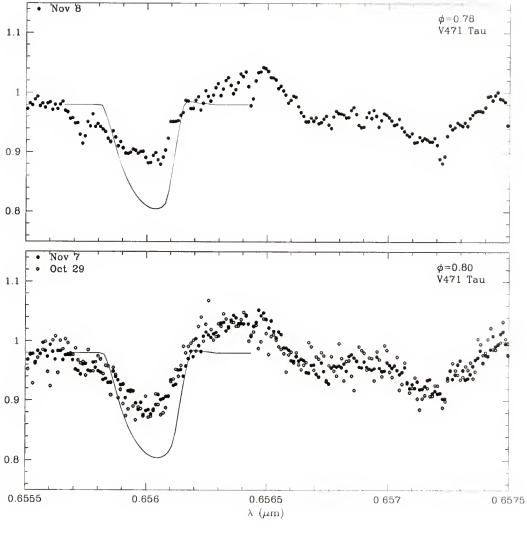

Figure 4.41: Observed spectra of V471 Tau (symbols) and the modeled Hα profile (solid line) for phases 0.78-0.80.

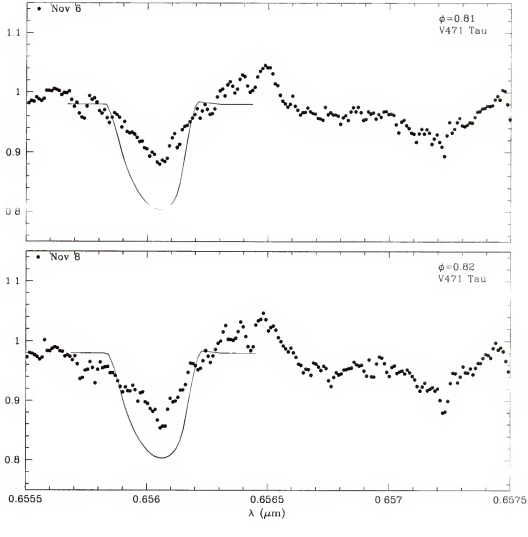

Figure 4.42: Observed spectra of V471 Tau (symbols) and the modeled Hα profile (solid line) for phases 0.81-0.82.

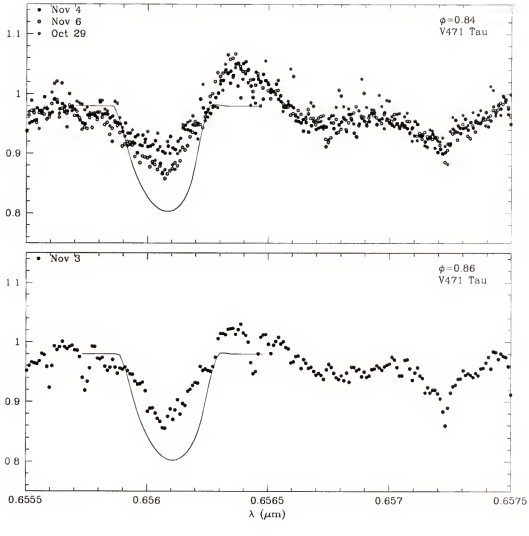

Figure 4.43: Observed spectra of V471 Tau (symbols) and the modeled Hα profile (solid line) for phases 0.84-0.86.

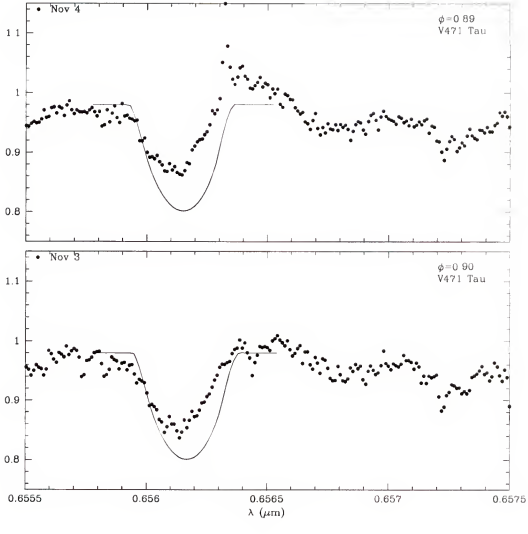

Figure 4.44: Observed spectra of V471 Tau (symbols) and the modeled Hα profile (solid line) for phases 0.89-0.90.

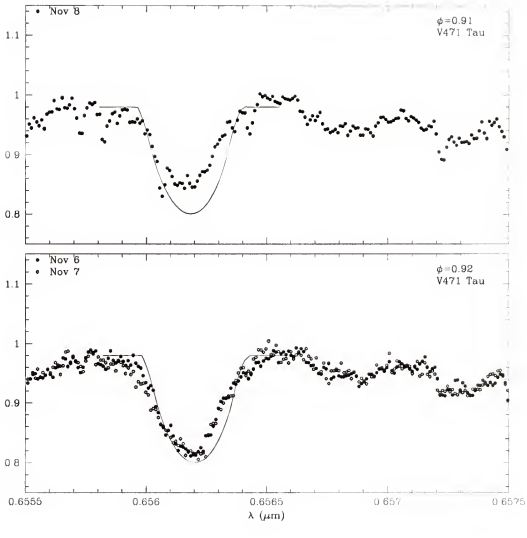

Figure 4.45: Observed spectra of V471 Tau (symbols) and the modeled Hα profile (solid line) for phases 0.91-0.92.

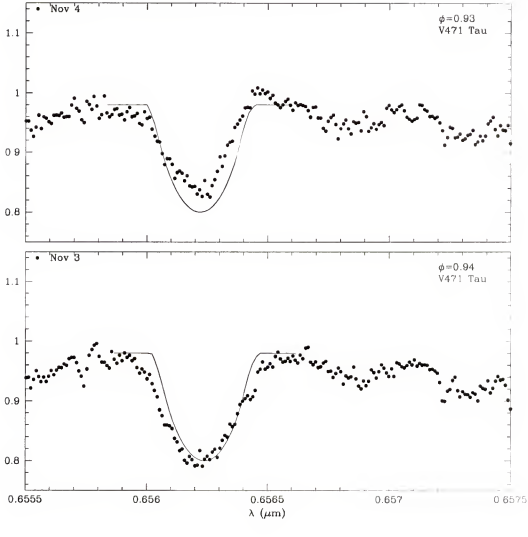

Figure 4.46: Observed spectra of V471 Tau (symbols) and the modeled Hα profile (solid line) for phases 0.93-0.94.

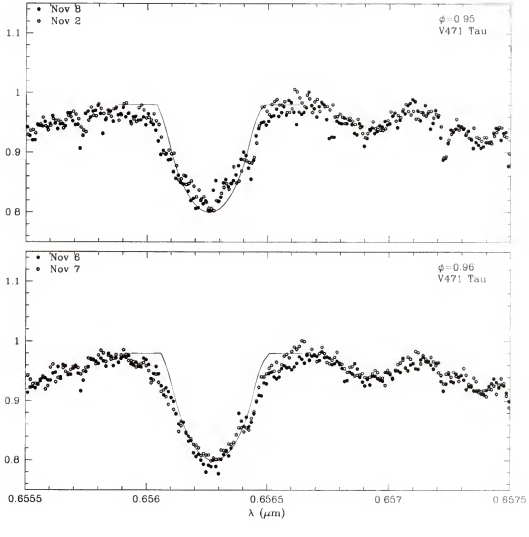

Figure 4.47: Observed spectra of V471 Tau (symbols) and the modeled Hα profile (solid line) for phases 0.95-0.96.

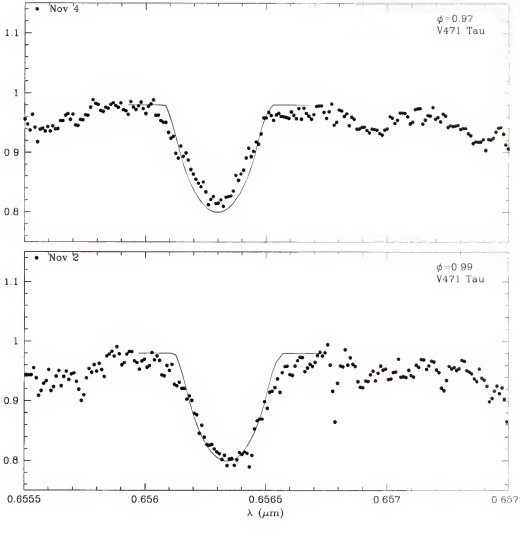

Figure 4.48: Observed spectra of V471 Tau (symbols) and the modeled Hα profile (solid line) for phases 0.97-0.99.

CHAPTER 5
CONCLUSION

We have presented simultaneous photometric and spectroscopic observations of the eclipsing binaries FF Aqr and V471 Tau. Light curves, radial velocities, and Hα profiles were analyzed with the WD program and orbital and stellar parameters were refined with the DC routine for both stars. A new ephemeris was found for FF Aqr with our radial velocities along with radial velocities and photometry from other authors. The secondary stars in both systems show distortions in their light curves, which are caused by dark spots. This means that we have caught these stars in a relatively high state of chromospheric activity. No flaring appears in our photometry but could have gone undetected since we did not cover the U band, where flares are most obvious.

Hα profiles for all phases observed were modeled as a fluorescent chromosphere on the secondary caused by incident UV radiation from a hot primary. We do see additional sources of Hα emission at high radial velocities, relative to the secondary star, which could be associated with the spots modeled in our light curves. Some distortions of the Hα profiles could have been caused by flaring that were caught by our half-hour exposure times. A persistent blue shifted excess seen in FF Aqr may be approaching material from some ejection event such as a coronal mass ejection.

We suggest that large extended structures (coronal loops) are magnetically anchored to spot regions and forced to co-rotate. When these structures are illuminated by the primary star they fluoresce and form the additional fast moving emissions seen in both stars. FF Aqr appears to have these structures located close to the sides facing the observer during quadrature, which gives rise to the overly broad Hα emission

seen at phase 0.5. V471 Tau shows an obvious excess that is close to the sub-stellar point. This excess appears blue shifted at phase 0.25, drifts across the line center of Hα, and reappears red shifted at phase 0.75. This emission is strongest at the beginning of our data and weakens over a couple of days but remains detectable over the 12 night observing run. Similar co-rotating structures have been seen in the rapidly rotating K dwarf AB Dor.

The level of emission due to chromospheric fluorescence is still uncertain for both stars. Contamination by extended structures prevents reliable calibration of the model's emission component from our data. We used the data at phase 0.25 for V471 Tau when the excess is Doppler shifted away from the stellar line for this calibration. If correct, it shows minimal emission above the continuum for a fluorescent chromosphere alone. The level of chromospheric fluorescence in FF Aqr is more uncertain because it is complicated by multiple structures and possibly emitting ejecta.

The prevalence of phase dependent Hα emission near phase 0.5 for both stars is still evident. The results shown here clearly indicate that multiple sources of emission are present, especially during times of high activity. New questions arise as to the mechanisms responsible for the observed excess emissions and their possible role in the orbital evolution of the stars. It becomes even more important to discover the extent of the emission from the fluorescent chromosphere, which should be a constant source, so that the transient sources can be better understood. More observations like those we obtained are needed at times of chromospheric quiescence. The apparent 12 year spot cycle of V471 Tau may provide us with just such an opportunity for the observing season of 2003.

REFERENCES

Baliunas, S.L., Loesser, J.G., Raymond, J.C., Guinan, E.F., Dorren, J.D. 1986, *In ESA Proceedings of an International Symposium on New Insights in Astrophysics. Eight Years of UV Astronomy with IUE* , (N87-19150 11-88), 185.

Barstow, M., Holberg, J., Cruise, A., Penny, A. 1997, *MNRAS* **290**, 505.

Beavers, W.I., Herczeg, T.J., Lui, A. 1986, *ApJ.* **300**, 785.

Bois, B., Lanning, H., Mochnacki, S. 1988, *AJ.* **96**. 157.

Bohm-Vitense, E. 1989, *Introduction to Stellar Astrophysics, Vol. 2*, 215.

Bopp, B.W. & Talcott, J.C. 1980, *AJ.* **85**, 55.

Bradstreet, D.H. 1993, *Binary Maker 2.0: Light Curve Synthesis Program*. Contact Software, (Norristown: Pennsylvania).

Cameron, A., Robinson, R. 1989a, *MNRAS* **236**, 57.

Cameron, A., Robinson, R. 1989b. *MNRAS* **238**. 657.

Clemens, J.C., Nather, R.E., Winget, D.E., Robinson, E.L., Wood, M.A., Claver, C.F., Provencal, J.,Kleinman, S.J., Bradley, P.A., Frueh, M.L., Grauer, A.D., Hine, B.P., Fontaine, G., Achilleos, N., Wickramasinghe,D.T., Marar, T.M.K., Seetha, S., Ashoka, B.N., O'Donoghue, D., Warner, B., Kurtz, D.W., Martinez, P., Vauclair, G., Chevreton, M., Barstow, M.A., Kanaan, A., Kepler, S.O., Augusteijn, T., van Paradijs, J., Hansen, C.J. 1992, *ApJ.* **391**, 773.

Donati, J.F., Collier Cameron, A., Hussain, G.A.J., Semel, M. 1999 *MNRAS* **302**, 437.

Dorren, J.D., Guinan E.F., Siah M.J. 1983, *IBVS* No. 2305.

Dworetsky, M.M., Lanning H.H., Etzel P.E., Patenaude D.J. 1977, *MNRAS* **181**. 13.

Etzel, P.B., Lanning, H.H., Dworetsky, M.M., Hamilton, I. 1988, *BAAS* **20** . 912.

Guinan, E.F., Wacker, S.W., Baliunas, S.L., Loeser, J.G., Raymond, J.C. 1986, *New Insights in Astrophysics: Eight Years of UV Astronomy with IUE*,(ESA SP-263), 197.

Guinan, E.F., Ribas, I. 2000, *ApJ* **546** . L43.

Guirado, J.C., Reynolds, J.E., Lestrade, J.F., Preston, R.A., Jauncey, D.L., Jones, D.L., Tzioumis, A.K., Ferris, R.H., King, E.A., Lovell, J.E., McCulloch, P.M., Johnston, K.J., Kingham, K.A., Martin, J.O., White, G.L., Jones, P.A., Arenou, F., Froeschlé, M., Kovalevsky, J., Martin, C., Lindegren, L., Söderhjelm, S. 1997, *ApJ.* **490**, 835.

İbanoğlu, C. 1989, *IBVS* No. 1088.

Lucy, L.B. 1995, *Zs.f.Ap* **65**, 89.

Marilli, E., Frasca, A., Bellina Terra, M., Catalano, S. 1995, *Astron. and Astrophys.* **295**, 393.

Martín, E.L., Pavlenko, Y., Rebolo, R. 1997, *Astron. and Astrophys.* **326** , 731.

Nelson, B., Young, A. 1970, *PASP* **82**, 699.

Oliver, J.P., Slovak, S.M., Africano, J. 1978, *IBVS* No. 1444.

Pringle, J.E., Wade, R.A. 1985, *Interacting Binary Stars*, 17.

Ramseyer, T., Hatzes, A., Jablonski, F. 1995, *AJ.* **110**, 1364.

Rottler, L., Batalha, C., Young, A., Vogt, S. 1998 *BAAS* **192** , 67.20.

Schaefer, K., Bond, H., Saffer, R., Sion, E. 1995 *BAAS* **187** , 18.04.

Skillman, D.R., Patterson, J. 1988 *AJ* **96** , 976.

Tunca, Z., Tümer, O., Kurutaç, M., İbanoğlu, C. 1979 *Ap&SS* **64** , 421.

Tunca, Z., Keskin, V., Evren, S., İbanoğlu, C. 1993 *Ap&SS* **204** , 297.

Van Hamme, W. 1993, *AJ.* **106**, 2096.

Wilson, R.E. 1979, *ApJ.* **234**, 1054.

Wilson, R.E. 1990, *ApJ.* **356**, 613.

Wilson, R.E., Devinney, E.J. 1971, *ApJ.* **166**, 605.

Wilson, R.E., Sofia, S. 1976, *ApJ.* **203**, 182.

Young, A., Lanning, H. 1975, *PASP* **87**, 461.

Young, A., Skumanich, A., Paylor, V. 1988, *ApJ.* **334**, 397.

Young, A., Rottler, L., Skumanich, A. 1991, *ApJ.* **378**, L25.

BIOGRAPHICAL SKETCH

Astronomy became a passion of mine while I was in the 3rd grade in Clearwater, Florida. I pursued my interest as an amateur for many years. I even attended a college night class at the St. Petersburg Community College when in the 5th grade. I decided to major in astronomy before attending college and chose Vanderbilt University for my undergraduate education. My research interests became focused in 1990 with my senior project at Vanderbilt where I received my B.S. in physics/astronomy in 1991. I worked with Dr. Fekel, with whom I measured radial velocities for the binary HD 30957. Other basic orbital parameters were then determined and I presented our findings at a seminar. This project, along with the resulting publication, was my initiation into the field of binary stars. During my second year at San Diego State University (1993), while working on my M.S. in astronomy, I was part of a project that included photometry of II Peg with the 21" telescope at Mount Laguna Observatory. The flare rate of this star was monitored at several observatories in a campaign initiated by Dr. P.B. Byrne of Armagh Observatory, Ireland. I wrote a FORTRAN program that modeled a variable spectral profile in the atmosphere of the cool component of the eclipsing binary V471 Tauri for my M.S. thesis. The thesis showed the need for additional observations along with a more realistic and rigorous model, which is the focus of this dissertation. I graduated in the summer of 1995 having been accepted to the University of Florida for work towards a Ph.D. and to work with Dr. Robert Wilson on binary stars.

In the spring of 1997 Dr. Wilson and I completed a project on the symbiotic binary, EG Andromedae. We analyzed light-curve data, which had been obtained by others over the past decade, and showed that an ellipsoidal variation of the giant star could explain the photometric observations. Our results were published in the *Monthly Notices of the Royal Astronomical Society*. In the summer of 1997 I held a research assistantship at BASF in Ludwigshafen, Germany, where I worked with Dr. Josef Kallrath who was completing the first definitive text on light-curve analysis of binary stars. While there I worked on a gas diffusion problem involving polymers. In the summer of 1999 I spoke about some of the preliminary results of my dissertation at a special Ph.D. conference in Kecskemét, Hungary.

I certify that I have read this study and that in my opinion it conforms to acceptable standards of scholarly presentation and is fully adequate, in scope and quality, as a dissertation for the degree of Doctor of Philosophy.

Robert E. Wilson , Chairman
Professor of Astronomy

I certify that I have read this study and that in my opinion it conforms to acceptable standards of scholarly presentation and is fully adequate, in scope and quality, as a dissertation for the degree of Doctor of Philosophy.

John P. Oliver
Associate Professor of Astronomy

I certify that I have read this study and that in my opinion it conforms to acceptable standards of scholarly presentation and is fully adequate, in scope and quality, as a dissertation for the degree of Doctor of Philosophy.

Charles M. Telesco
Professor of Astronomy

I certify that I have read this study and that in my opinion it conforms to acceptable standards of scholarly presentation and is fully adequate, in scope and quality, as a dissertation for the degree of Doctor of Philosophy.

Francisco J Reyes
Associate Professor of Astronomy

I certify that I have read this study and that in my opinion it conforms to acceptable standards of scholarly presentation and is fully adequate, in scope and quality, as a dissertation for the degree of Doctor of Philosophy.

Michael J Kaufman
Professor of Materials Science
and Engineering

This dissertation was submitted to the Graduate Faculty of the Department of Astronomy in the College of Liberal Arts and Sciences and to the Graduate School and was accepted as partial fulfillment of the requirements for the degree of Doctor of Philosophy.

May 2001

Dean, Graduate School